Invited paper

OPTO-ELECTRONICS REVIEW **8**(1), 1–24 (2000)

Photoreflectance spectroscopy of low-dimensional semiconductor structures

J. MISIEWICZ*, P. SITAREK, and G. SĘK

Institute of Physics, Wrocław University of Technology
27 Wybrzeże St. Wyspiańskiego, 50-370 Wrocław, Poland

In this paper, we present the applications of photoreflectance spectroscopy for investigations of low-dimensional, semiconductor structures. We briefly introduce the theoretical background of this technique including the line-shape expressions related to semiconductor microstructures. We show examples of photoreflectance investigations of two-dimensional structures such as quantum wells, multiple quantum wells and superlattices, one-dimensional structures – quantum wires, and quasi zero-dimensional structures – quantum dots. Finally, we concentrate our attention on investigations of the structures of semiconductor devices like high electron mobility transistors, heterojunction bipolar transistors and vertical/planar light emitting laser structures.

Keywords: photoreflectance, low-dimensional heterostructures, transistors, semiconductor lasers.

1. Introduction

Because of their novel physical properties and device applications, new materials and based on them semiconductor heterostructures such as quantum wells (QWs), multiple quantum wells (MQWs), superlattices (SLs), and heterojunctions have been produced. To explore various physical properties of these structures, number of characterisation methods, including photoluminescence (PL), photoluminescence excitation (PLE) spectroscopy, transmission electron microscopy (TEM), X-ray techniques, Hall measurements, etc., have been applied. Most of the above methods require special conditions such as low temperatures (PL, PLE), or special sample preparation (TEM, Hall measurements). For practical applications, it is advantageous to have a technique, which is simple and at the same time provides a lot of useful information. Such is photoreflectance (PR), a contactless modulation spectroscopy technique. This method was proposed in the sixties and was used in investigations of semiconductor band structure parameters in the seventies.

Glembocki *et al.* in 1985 [1] reported the first application of this technique to semiconductor microstructures studies. Because of its extreme sensitivity to interband electronic transitions, many papers on this subject have been published since 1985. This sensitivity to interband electronic transitions is due to the derivative nature of the measurements [2]. Another important feature of photoreflectance is that the measurements can be carried out even at room temperature, still providing as much information as other methods (PL, PLE) at very low temperatures. By using photoreflectance at 300 K, it is possible to determine the interband transition energies in semiconductor microstructures (QWs, MQWs, and SLs) or device structures (i.e., transistors or lasers) with an accuracy of a few meV.

A number of review papers about the application of photoreflectance spectroscopy to the investigation of semiconductors and semiconductor structures has been published up to now [2–6].

In this paper, we present the applications of photoreflectance spectroscopy for investigations of both low-dimensional, semiconductor structures, and semiconductor device structures. We briefly introduce the theoretical background of the technique and line-shape formulas associated with semiconductor microstructures. We show examples of PR spectroscopy applications for studies of two-dimensional (QWs, MQWs, and SLs), one-dimensional (quantum wires) and zero-dimensional (quantum dots) structures. Finally, we turn our attention to investigations of semiconductor device structures such as transistors and semiconductor lasers.

2. Principles of photoreflectance spectroscopy

A derivative of an optical spectrum (i.e., the reflectivity) with respect to some parameter is evaluated with any modulation spectroscopy. The measured optical signal depends on the joined density of states making this method sensitive to transitions at the critical point in the Brillouin zone of the studied material. The resulting spectrum has sharp, derivative-like features on a featureless background. The modulation can easily be accomplished by varying some

*e-mail: jmis@if.pwr.wroc.pl

parameters, associated with the sample or the experimental system, in a periodic fashion and measuring the corresponding normalised change in the optical properties. It is possible to modulate a variety of parameters, i.e., the wavelength of light, the temperature, the applied stress or the electric field in the studied sample. The electromodulation techniques are based on the modulation of the electric field. One of the electromodulation techniques is photoreflectance spectroscopy where the varying parameter is the internal (built-in) electric field.

Modulation of the electric field in the sample is caused by photo-excited electron-hole pairs created by the pump source (usually laser) which is chopped with a given frequency. The photon energy of the pump source is generally above the band gap of the semiconductor being under study. There is a possibility to use a below band-gap modulation through the excitation of impurity or surface states [7].

Recently, Pollak [5], Glembocki and Shanabrook [2] have provided a most detailed theoretical background of the photoreflectance technique.

2.1. Line-shapes

The chopped laser light affects periodically the built-in electric field. The perturbation, due to the changes of electric field, causes modulation of the complex dielectric function ε ($\varepsilon = \varepsilon_1 + i\varepsilon_2$) of structure under investigation. Changes in the dielectric function are directly connected with the changes of the optical response of the structure, i.e., reflectivity. The relative changes of the reflectivity $\Delta R/R$ can be written as [8]

$$\frac{\Delta R}{R} = \alpha_s(\varepsilon_1,\varepsilon_2)\Delta\varepsilon_1 + \beta_s(\varepsilon_1,\varepsilon_2)\Delta\varepsilon_2 , \qquad (1)$$

where α_S and β_S are the Seraphin coefficients, related to the unperturbed dielectric function, and $\Delta\varepsilon_1$ are $\Delta\varepsilon_2$ the changes in the complex dielectric function due to the perturbation. The quantities $\Delta\varepsilon_1$ and $\Delta\varepsilon_2$ are related by the Kramers-Kronig relations.

Electromodulation can be classified into three categories depending on the relative strengths of characteristic energies [9]. In the low-field regime $|\hbar\Theta| \leq \Gamma$ where $\hbar\Theta$ is the electro-optic energy given by

$$(\hbar\Theta)^3 = \frac{e^2\hbar^2F^2}{2\mu}. \qquad (2)$$

In the above equation, F is the electric field, μ is the reduced interband mass in the direction of the field. When $|\hbar\Theta| \leq \Gamma$ but $eFa_0 << E_g$ (a_0 is the lattice constant and E_g is the band gap energy) it is the intermediate-field case. In this case, the Franz-Keldysh oscillations (FKO) appear in the spectrum. In the high-field regime the electro-optic energy is much greater than the broadening but $eFa_0 \approx E_g$ so that Stark shifts are produced.

2.1.1. Third-derivative spectroscopy in low-field limit

The perturbation, due to the modulation of the electric field, destroys the translational symmetry and hence can accelerate free charge carriers in the crystal [10,11]. In effect, under certain electric field conditions, electromodulation results in sharp, third-derivative line-shapes.

For Lorenzian form of the dielectric constant, low-field modulation, and under a parabolic band approximation, one can rewrite Eq. (1) as [9]

$$\frac{\Delta R}{R} = \mathrm{Re}\left[Ae^{i\varphi}(E - E_g + i\Gamma)\right]^{-m}, \qquad (3)$$

where Γ is the broadening parameter ($\Gamma \sim \hbar/\tau$), A and φ are the amplitude and phase factor, respectively. The parameter m in the line-shape factor of Eq. (3) depends on the type of the critical point. In a three-dimensional system, m equals 2.5 while for a two-dimensional critical point m = 3.

2.1.2. First-derivative spectroscopy in the low electric field limit

The perturbation due to the changes of the electric field does not accelerate charge carriers in their bound states such as excitons, quantum wells or impurities. These types of particles are confined in space, which does not have a translational symmetry. For bound states the photoreflectance line-shape has first-derivative character [12], and the changes in the dielectric function may be expressed as

$$\Delta\varepsilon = \left[\frac{\delta\varepsilon}{\delta E_g}\frac{\delta E_g}{\delta F_{AC}} + \frac{\delta\varepsilon}{\delta\Gamma}\frac{\delta\Gamma}{\delta F_{AC}} + \frac{\delta\varepsilon}{\delta I}\frac{\delta I}{\delta F_{AC}}\right]F_{AC}, \qquad (4)$$

where F_{AC} is the change in the built-in electric field and I is the intensity of the optical transition. Equation (4) can be rewritten as [13]

$$\Delta\varepsilon_i = \left[A_E f_E^i + A_\Gamma f_\Gamma^i + A f_I^i\right]\frac{I}{\Gamma}F_{AC}, \quad i = 1,2, \qquad (5)$$

with

$$A_E = \frac{1}{\Gamma}\frac{\delta E_g}{\delta F_{AC}}, \qquad f_E^i = \frac{\delta\varepsilon_i}{\delta E_g},$$
$$A_\Gamma = \frac{1}{\Gamma}\frac{\delta\Gamma}{\delta F_{AC}}, \quad \textit{and} \quad f_\Gamma^i = \frac{\delta\varepsilon_i}{\delta\Gamma}, \qquad (6)$$
$$A_I = \frac{1}{I}\frac{\delta I}{\delta F_{AC}}, \qquad f_I^i = \frac{\delta\varepsilon_i}{\delta I}.$$

Depending on the broadening mechanism (i.e., temperature), the unperturbated dielectric function can be either Lorenzian or Gaussian. For quantum wells, the dielectric

 © 2000 COSiW SEP, Warsaw

function is excitonic, even to elevated temperatures. Thus for the quantum microstructures, the Lorenzian or Gaussian profile of dielectric function is appropriate. The Lorenzian dielectric function can be written as [11]

$$\varepsilon = 1 + \frac{I}{E - E_g + i\Gamma}. \tag{7}$$

The modulation terms of Eq. (5) are given by

$$\begin{aligned} f_E^1 &= \frac{y^2 - 1}{(y^2+1)^2}, \quad f_\Gamma^1 = f_E^2, \quad f_I^1 = \frac{y}{y^2+1}, \\ f_E^2 &= \frac{-2y}{y^2+1}, \quad f_\Gamma^2 = -f_E^1, \quad f_I^2 = \frac{-1}{y^2+1}, \end{aligned} \tag{8}$$

where

$$y = \frac{E - E_g}{\Gamma}. \tag{9}$$

If the intensity modulation terms are ignored, only two independent line-shape factors [see Eq. (8)] do not vanish. The combined spectral dependence can then be expressed by Eq. (3) with m = 2 [11].

The unperturbated dielectric function of a Gaussian profile is given by [13]

$$\varepsilon = 1 + I(L_1 + iL_2), \tag{10}$$

where

$$\begin{aligned} L_1 &= \frac{y}{\Gamma}\Phi(1,3/2 - y^2/2), \\ L_2 &= \sqrt{\frac{\pi}{2}}\frac{1}{\Gamma}\exp(-y^2/2). \end{aligned} \tag{11}$$

Φ is the confluent hypergeometric function. In this case the modulation terms of Eq. (5) can be written as

$$\begin{aligned} f_E^1 &= -\Phi(1,1/2,-y^2/2), \\ f_E^2 &= -\sqrt{\frac{\pi}{2}}y\exp(-y^2/2), \\ f_\Gamma^1 &= -2y\Phi(2,3/2,-y^2/2), \\ f_\Gamma^2 &= -\sqrt{\frac{\pi}{2}}(y^2-1)\exp(-y^2/2), \\ f_I^1 &= y\Phi(1,3/2,-y^2/2), \\ f_I^2 &= -\sqrt{\frac{\pi}{2}}\exp(-y^2/2). \end{aligned} \tag{12}$$

In Fig. 1, various modulation terms of Eq. (12) are plotted. Some of the profiles from Fig. 1 look quite similar to each other (i.e. f_E^1 and $-f_\Gamma^2$). If f_I^1 and f_I^2 are ignored, only two line-shape profiles can be used to fit experimental data. Hence, for the dielectric function of Gaussian type one can get

$$\frac{\Delta R}{R} = Af_E^1 + Bf_E^2. \tag{13}$$

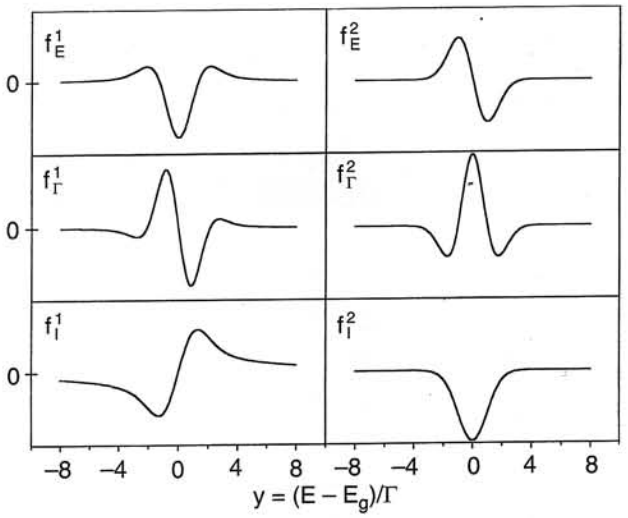

Fig. 1. Calculated line shapes for the derivatives of the real and imaginary parts of a Gaussian dielectric function.

2.1.3. The Franz-Keldysh oscillations

When the low-field criteria are not satisfied, but $eFa_0 << E_g$, the dielectric function can exhibit Franz- -Keldysh oscillations. Although the exact form of $\Delta R/R$ for the intermediate-field case with the broadening is quite complicated, Aspnes and Studna [14] have derived a relatively simple expression

$$\begin{aligned} \frac{\Delta R}{R} \propto \frac{1}{E^2(E-E_g)^{1/2}} &\exp\left[-2(E-E_g)^{1/2}\frac{\Gamma}{(\hbar\Theta)^{3/2}}\right] \\ &\times \cos\left[\frac{4}{3}\frac{(E-E_g)^{3/2}}{(\hbar\Theta)^{3/2}} + \chi\right]. \end{aligned} \tag{14}$$

From the above equation, the position of the n^{th} extreme in the Franz-Keldysh oscillations is given by

$$n\pi = \frac{4}{3}\left[\frac{E_n - E_g}{\hbar\Theta}\right]^{3/2} + \chi, \tag{15}$$

where E_n is the photon energy of the n^{th} extreme and χ is an arbitrary phase factor [15].

2.2. Experimental details

In Fig. 2, a schematic diagram of the photoreflectance apparatus is shown. The probe light is a monochromatic beam obtained from a quartz halogen lamp dispersed through a monochromator. This beam (of intensity I_0) is focused on the sample. The laser pumping beam illuminates the same spot of the sample. The laser beam is chopped with frequency of few hundreds Hz. The photon energy of the pump source should be generally above the band gap of the

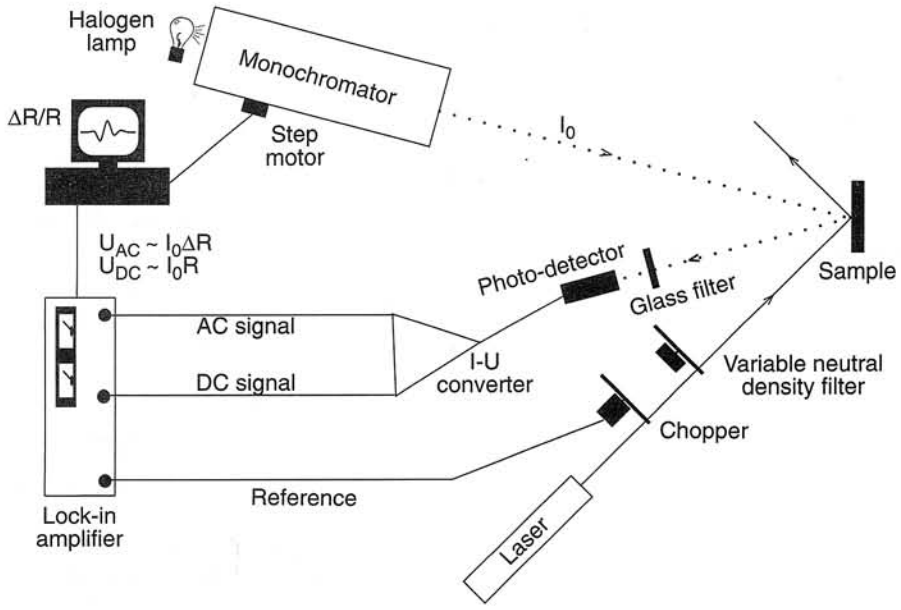

Fig. 2. Schematic diagram of photoreflectance apparatus.

semiconductor being investigated. A He-Ne laser (the energy range below 1.96 eV) or Ar^+ ion laser (the energy range below 4.5 eV) is used as a typical pump source. The intensity, of the laser light can be adjusted by a variable, neutral density filter. The light reflected from the sample is detected by a photodiode or a photomultiplier. In order to prevent the detection of laser light, an appropriate longpass glass filter is used in front of the photo-detector. The current-voltage converter, connected to the detector, separates the signal into two components. The DC component is proportional to I_0R, and AC component is proportional to $I_0\Delta R$. The AC component is measured in a lock-in amplifier. A computer divides the AC signal by the DC component giving the photoreflectance spectrum, $\Delta R/R(\hbar\omega)$.

3. Photoreflectance study of low-dimensional semiconductor structures

3.1. Quantum wells, multiple quantum wells and superlattices

Since the middle of sixties, the modulation spectroscopy techniques have proved its high applicability for studying and characterising the properties of bulk semiconductors. During the first decade, the method was recognised as a new, high-resolution technique for the solid state spectroscopy [9,11,16].

In the eighties, modulation spectroscopy had a renaissance. The advantages exploited for bulk studies were applicable also in the semiconductor microstructures fabricated by MBE or MOCVD such as QWs, MQWs or SLs. In 1985, Glembocki *et al.* [1] showed that multiple quantum wells, grown on semi-insulating substrates, could be studied by the photoreflectance technique.

Line-shape analysis, based on Eqs. (3), (13), and (14) (we will call it further fitting procedure) is an integral aspect of photoreflectance spectroscopy. These procedures allow analysing the complicated photoreflectance spectra in terms of the theoretical parameters. Thus, the fitting provides valuable information about the energy gaps and line widths associated with the optical transitions.

A photoreflectance spectrum (dotted lines) of a GaAs/AlGaAs MQW structure (with a well width of 20 nm) at temperatures 6 K, 77 K and 150 K in the region of the 11H and 11L feature [6,17] is shown in Fig. 3. The solid and dashed lines are fits to the first-derivative of Lorenzian (first derivative Lorenzian line shape – FDLL) and Gaussian (first derivative Gaussian line shape – FDGL) profiles, respectively. At 6 K, the fit of the Lorenzian profile to the data is very good. At 77 K, the data cannot be adequately represented by either profile. An intermediate profile is required to fit the data. A Gaussian dielectric function results in nearly perfect fit at 150 K.

For quantum wells, because of the enhanced exciton binding energy caused by the reduced dimensionality, the dielectric function has an excitonic character even at elevated temperatures. At the elevated temperatures, the dielectric function broadening, caused by strong exciton-phonon interaction, impurities and defects, changes the absorption profile of excitons from Lorenzian to Gaussian. Thus, at high temperatures, a Gaussian profile of dielectric function must be used to fit the experimental data. At low temperatures, a Lorenzian dielectric function is more appropriate. Between 50 K and 150 K the transition from Lorenzian to Gaussian is not abrupt and the line shapes are of an intermediate form between Lorenzian and Gaussian. Equation (3) with parameter m = 3 (2D critical point) sometimes is used to reflect the FDGL, providing a reasonable fit to the room-temperature experimental data.

 © 2000 COSiW SEP, Warsaw

At the beginning, single QW or MQW structures received the most attention in PR studies. In MQW structures, the barrier layer is thick enough to prevent significant wave function overlap between wells.

Room temperature spectra for several MQW structures and thick heterostructure of GaAs and AlGaAs layers (for comparison) obtained by Glembocki *et al.* [1], are shown in Fig. 4. In the top spectrum, two resonances corresponding to the direct band-gaps of GaAs (low-energy resonance) and AlGaAs (high-energy resonance) are visible. The other spectra were obtained for MQW structures with quantum wells width of 15 nm, 24 nm, and 46 nm. The arrows indicate the energies of the allowed quantum well transitions. The notation mnH (mnL) represents the QW optical transition between the m^{th} electron subband in the conduction band and the n^{th} heavy (light) hole subband in the valence band. It is worth to note that at room temperature Glembocki *et al.* observed up to nine transitions in QWs.

In addition to parity allowed transitions ($m - n = 0, \pm 2, \pm 4, ...$) it has been shown that parity forbidden transitions can be observed in QWs. The selection rules may be broken, i.e., by nonparabolicities in the valence band states and by electric field (internal and external).

Allowed and forbidden optical transitions in a GaAs/AlGaAs MQW structure was also studied by Sitarek *et al.* [18]. The structure was grown by the MBE on (001) GaAs substrate. The MQW under investigations consisted of 60 periods of GaAs and $Al_{0.35}Ga_{0.65}As$ layers with thickness of 15 nm each. Measured at room temperature PR spectrum had a very rich structure. In order to identify all features, PR measurement was also carried out at a liquid nitrogen temperature. The obtained PR spectrum is shown in Fig. 5. The arrows indicate the intersubband transitions. Both, the symmetry allowed and forbidden transitions are marked in the figure. A small, built-in electric field is probably responsible for the presence of 21H, 23H and 21L symmetry forbidden transitions in the spectrum. These transitions are much weaker than the symmetry allowed transitions. Because of the finite depth of the well, the 13H transition is parity allowed and its intensity is comparable to the symmetry allowed transitions. Optical transitions involving unconfined states are present above the feature corresponding to the band gap of AlGaAs [19]. The energies of present in the spectrum resonances, were accurately determined by Sitarek *et al.* through a fit of the first derivative Gaussian line shape function, Eq. (13), to the experimental data.

In order to identify the nature of the large number of intersubband transitions observed in the MQW, Sitarek *et al.* have performed a theoretical calculation based on the envelope function approximation [20]. The energy values obtained from this calculation agree very well with the experimental data.

The temperature dependence of both the energy and broadening of interband electronic transitions can yield important information about, e.g., electron-phonon interactions or excitonic effects. An increase of temperature leads to a red shift of the band gaps and an increase in the line

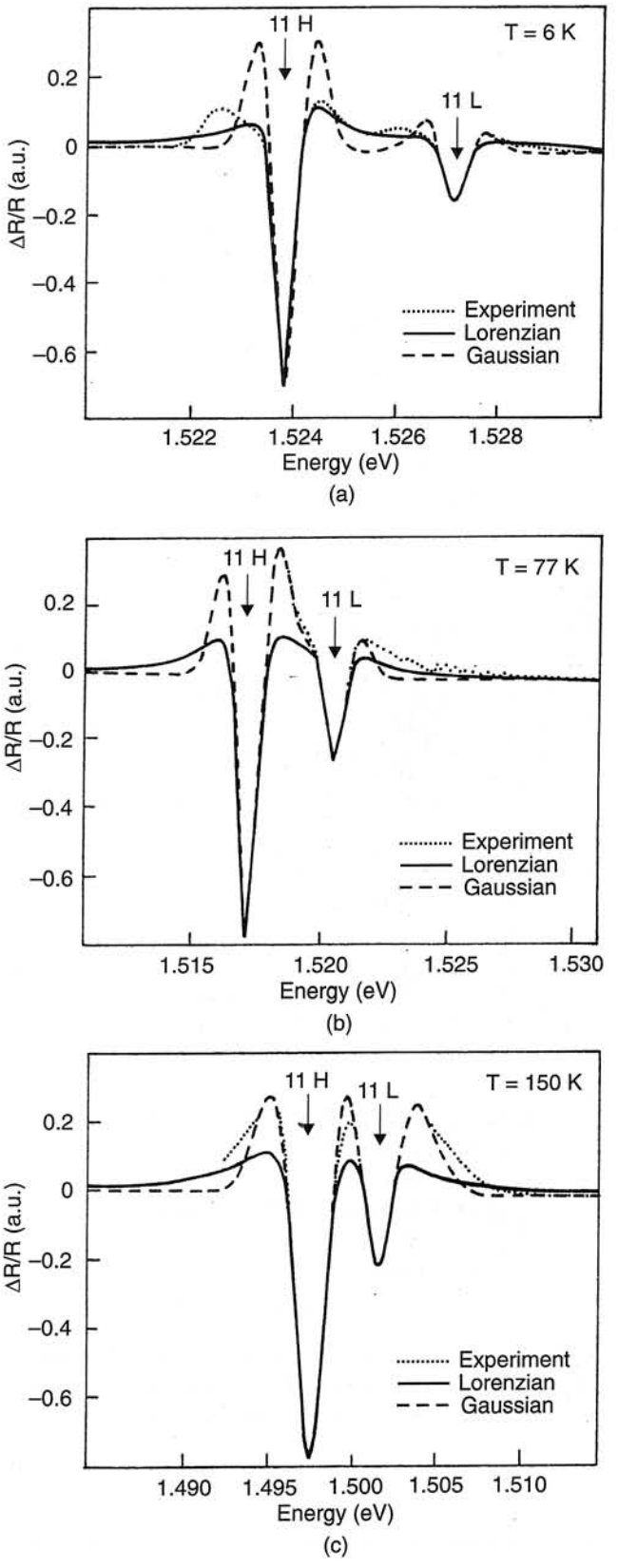

Fig. 3. Photoreflectance spectra (dotted line) at different temperatures from GaAs/AlGaAs MQW structure. First derivative Lorenzian (solid lines) and Gaussian (dashed lines) line shapes are compared (after Ref. 6).

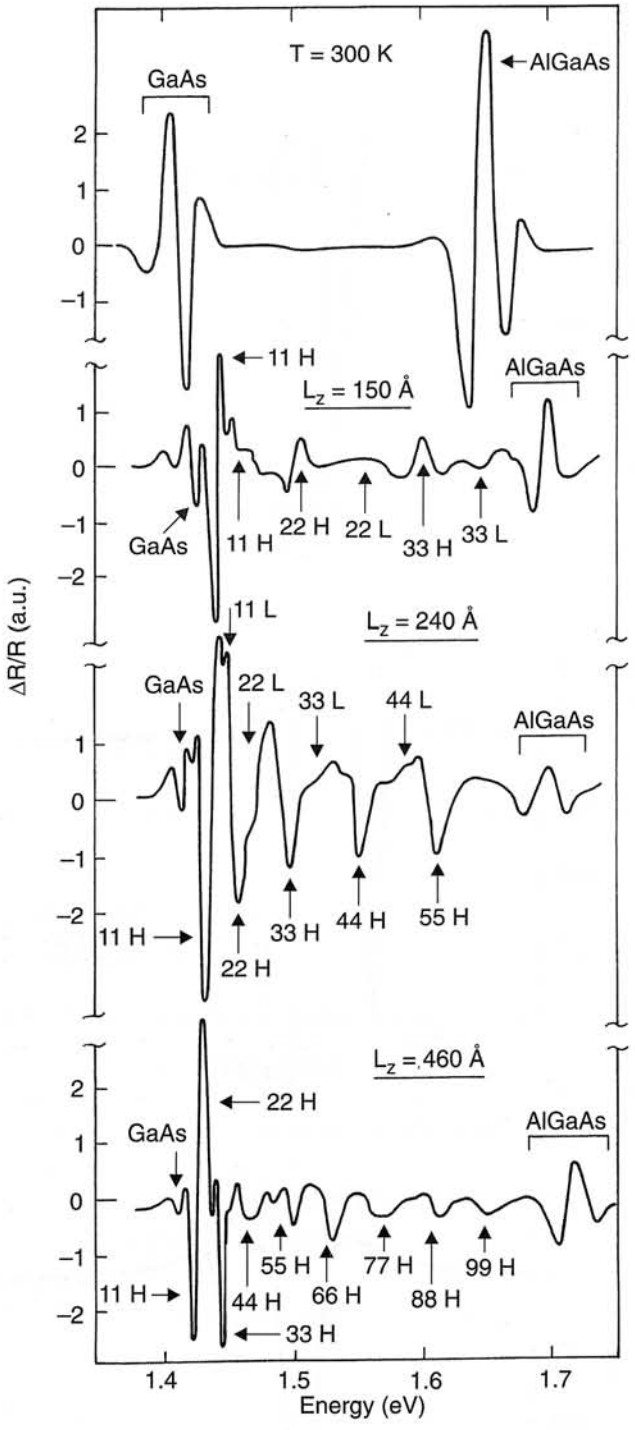

Fig. 4. Room temperature PR spectra for three GaAs/AlGaAs MQWs with different well width L_z, and spectrum for thick AlGaAs/GaAs heterostructure (after Ref. 1).

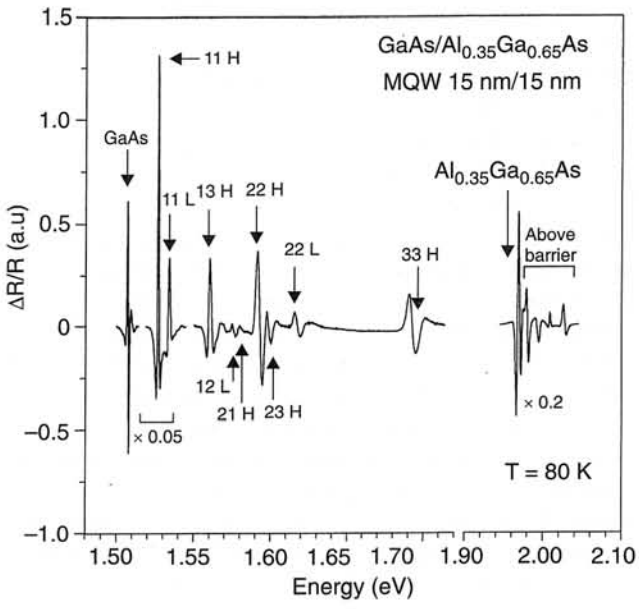

Fig. 5. Photoreflectance spectrum of $GaAs/Al_{0.35}Ga_{0.65}As$ MQW with wells and barriers of 15 nm width measured at 80 K. The arrows indicate optical transition energies obtained from the theoretical calculation (after Ref. 18).

Sitarek *et al.* have [18] reported a study of the temperature dependence of PR spectra from $Al_{0.35}Ga_{0.65}As/GaAs$ MQW in the 80 K to 300 K temperature range. In Fig. 6, the PR spectra of the 11H and the 11L transitions at different temperatures are shown. From the least-squares fits to the experimental data with FDGL the values of E_{11H} were obtained. The fit also yielded the broadening parameter Γ.

The parameters in the Bose-Einstein expression

$$E(T) = E_B - a_B\left\{1 + 2/[\exp(\Theta_B/T) - 1]\right\} \qquad (16)$$

such as the strength of the electron-phonon interaction a_B, and the corresponding to the average phonon temperature Θ_B, describe the temperature dependence of 11H transition energies of AlGaAs/GaAs MQW. From the obtained data, E_B = 1.588 eV, a_B = 56 meV and Θ_B = 247 K. For bulk GaAs, these parameters are E_B = 1.571 eV, a_B = 57 meV, and Θ_B = 240 K. The values of a_B and Θ_B, obtained for 11H transition, are very similar to values for bulk GaAs. In the lattice matched AlGaAs/GaAs heterostructures, the temperature dependence of the band gap of the material forming the wells is the main factor affecting the relation of the transition energy and temperature.

The variation of the broadening parameter with temperature can also be expressed by a Bose-Einstein expression

$$\Gamma(T) = \Gamma_0 + \Gamma_1/\left[\exp(E_{ph}/kT) - 1\right] \qquad (17)$$

where Γ_0 contains inhomogeneity contribution resulting from the interface roughness, alloy clustering and strain distribution (a small value of Γ_0 tells us that structure is

width. The temperature variation of the energy gaps can be described by equations involving three parameters such as the Varshni expression or the more recently proposed term containing the Bose-Einstein occupation factor for phonons [5]. A similar Bose-Einstein equation also has been used to fit the temperature dependence of the broadening function.

 © 2000 COSiW SEP, Warsaw

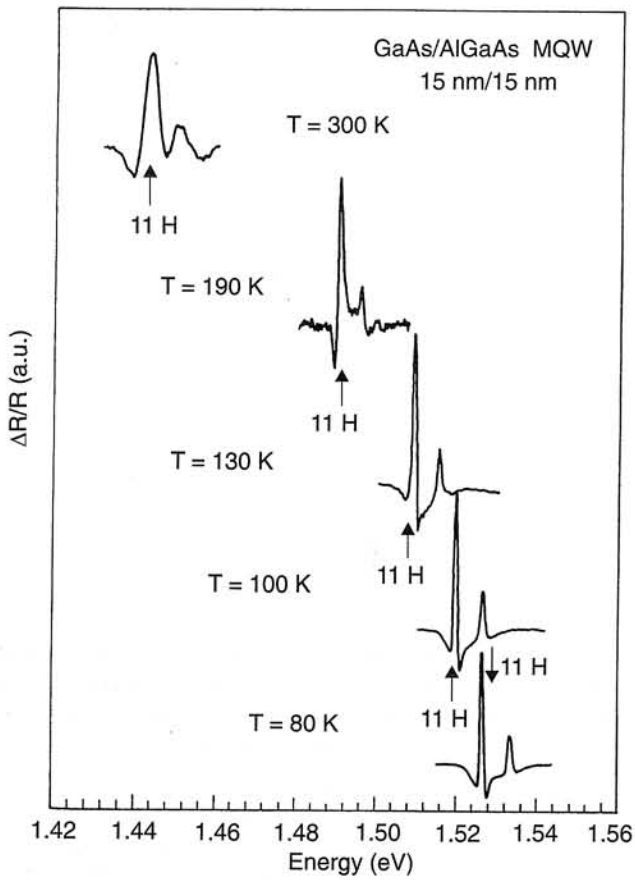

Fig. 6. Measured at different temperatures the photoreflectance spectra of GaAs/$Al_{0.35}Ga_{0.65}As$ MQW structure in the energy range of 11H and 11L transitions. The intensities of transitions at different temperatures are not in scale. Vertical lines mark 11H transition energy (after Ref. 18).

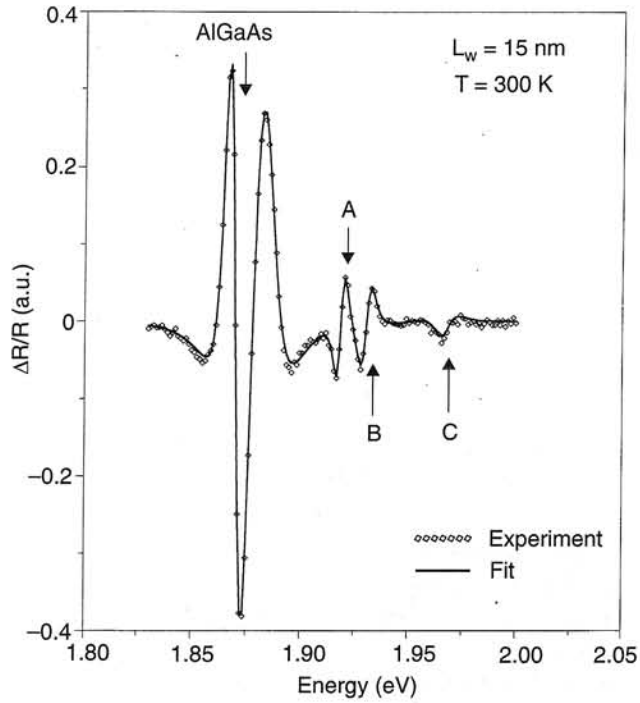

Fig. 7. Photoreflectance spectrum of GaAs/$Al_{0.35}Ga_{0.65}As$ MQW structure in the range above the barrier transitions. Dotted line is the experimental curve. Solid line is the fit according to Eq. 4. Arrows mark the energies of optical transitions involving unconfined states (after Ref. 19).

very homogeneous); parameter Γ_1 represents the strength of electron-phonon coupling; E_{ph} is the energy of the longitudinal optical phonon (36 meV for GaAs). For the 11H transition, Sitarek *et al.* found that $\Gamma_0 = 0.71$ meV.

In studies of electronic and optical properties of quantum wells (and multiple quantum wells), the major attention has been focused on confined states. In quantum well structures, the existence of energy levels formed above (below) the conduction (valence) band of the barriers has been observed in both low temperature Raman spectroscopy [21] and low temperature PLE spectroscopy [22]. Using photoreflectance spectroscopy it is possible to investigate optical transitions involving the unconfined states at room temperature [23,24]. Up to now the little work has been done on the study of such subbands.

The features observed at energies higher than the resonance corresponding to bulk AlGaAs seen in Fig. 5 were under detailed study by Sitarek et al. [19]. A room temperature PR spectrum for an $Al_{0.35}Ga_{0.65}As$/GaAs MQW with a 15 nm well width, is shown in Fig. 7 for the energies equal and higher than the band gap of the barrier energy. The feature at about 1.87 eV corresponds to the direct band gap of AlGaAs. Three additional features, marked A, B, and C, were observed above the resonance related to AlGaAs band gap.

Sitarek *et al.* reported energy level splitting in the optical transitions between unconfined electron and hole subbands in AlGaAs/GaAs MQWs. The splitting is associated with the energy dispersion in the direction along the MQW growth direction (z axis). This dispersion leads to the formation of subbands in superlattices (and MQW structures). The width of the subband is determined by the energy difference between the quantised state at $k_z = 0$ (Brillouine zone centre) and $k_z = \pi/d$ (Brillouine zone edge). Here $d = L_W + L_B$ is the sum of the well thickness L_W and the barrier thickness L_B.

In order to obtain the transition energies between subbands, the third-derivative functional form – Eq. 3, [11,25] was used to fit the PR experimental data. The solid line in Fig. 7 shows the least squares fit to the third-derivative functional form (TDFF). The optical transitions energies obtained from the fitting procedures are listed in Table 1. The notation m-nH/L (Γ/π) denotes transitions between the m^{th} conduction subband to n^{th} valence subband corresponding to heavy (H) or light (L) holes, while Γ (or π) means that the transition occurs in Brillouine zone (BZ) centre (or BZ edge).

The transition energy values, obtained from using the envelope function theoretical model, are listed in Table 1 in the column named "Theory". Only the symmetry allowed m = n transitions were analysed.

Table 1. Experimental and theoretical values of the unconfined optical transitions of MQW structure with well width of 15 nm. The capital letters A, B and C indicates the features present in the figure.

Transition	Experiment	Theory
6-6H (π)		1.891
5-5L (Γ)		1.901
6-6H (Γ)	1.919 (A)	1.918
5-5L (π)	1.930 (B)	1.942
7-7H (Γ)		1.949
6-6L (π)	1.968 (C)	1.959
7-7H (π)		1.985

As it can be seen in Table 1, the first feature, marked in Fig. 7 as A, originates from the optical transition between the sixth electron subband and the sixth heavy hole subband at the BZ centre [6-6H(Γ)]. There is a very good agreement between energy values obtained from the experiment and the theory. Enumeration of transitions is continuos and starts with transitions confined in the wells. Unconfined transitions start with the number six for heavy holes and five for light holes (for structure with well width of 15 nm). Agreement between the experimental and theoretical energy values for the next two features, B and C, is worse than for A feature. In that energy region there are four allowed transitions: 5-5L (π), 6-6L (π) and a split 7-7H transition making the identification of B and C features difficult.

In strained systems, the properties of the electron and hole quantum states depend on both the strain and quantum confinement. It is useful to define the conduction band offset parameter

$$Q_C = \Delta E_C / (\Delta E_C + \Delta E_V^{HH}), \qquad (18)$$

where ΔE_c and ΔE_V^{HH} are the conduction band and the heavy-hole valence band discontinuities, respectively. When a thin InGaAs layers are grown on a AlGaAs buffer layer, a biaxial in-plane compression and a corresponding extension (tensile strain) along the growth direction are sustained in InGaAs. Such a strain alters the band structure of InGaAs [26]. The energy band gap increases due to the compressive hydrostatic component of the strain while the tensile, (001) uniaxial strain splits the heavy-light hole degeneracy at the Brillouine zone centre. The relative positions of the bands in the InGaAs/GaAs QWs can lead to two possible configurations of the potential of the well. If the conduction band offset parameter Q_C is less than 0.5, both the electrons and the holes are confined to the InGaAs region. In the other case ($Q_C > 0.5$), the electrons and the heavy holes are in the InGaAs region (type I configuration), while the light holes are in the GaAs region (type II configuration).

Sęk *et al.* [27] studied InGaAs/GaAs QW structure grown by MOCVD. The structure consisted of five 10 nm $In_{0.115}Ga_{0.885}As$ quantum wells separated with 80 nm GaAs barriers. In Fig. 8, the PR spectrum of this structure is shown. Three features are present in the spectrum. The highest energy resonance originates from both the cap and the buffer GaAs layers. The two lower energy features correspond to the optical transitions in the QWs. Comparing the transition energy values, obtained from experiment (line shape analysis with FDGL) and from theoretical calculations (based on an envelope approximation [20] including strains and the exciton binding energies) Sęk *et al.* found that the feature at about 1.33 eV corresponds to 11H transition and the feature at about 1.37 eV corresponds to 11L optical transition. They also concluded that light holes are confined in GaAs layer – type II configuration.

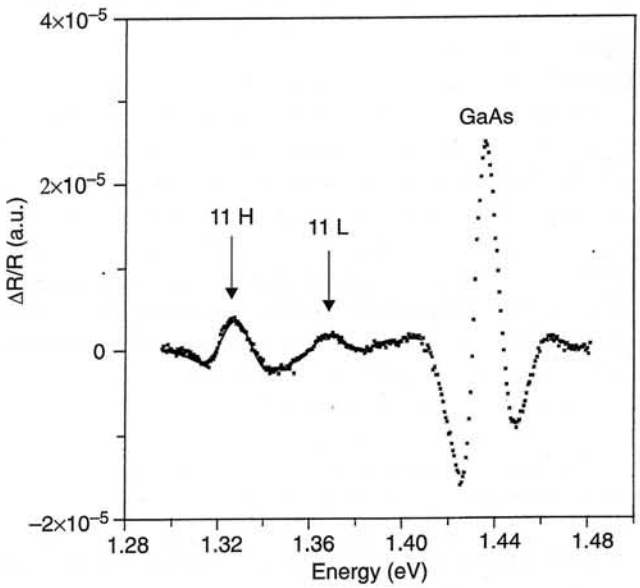

Fig. 8. The room temperature PR spectrum (dotted line) from $In_{0.115}Ga_{0.885}As$/GaAs MQW structure. Solid line is first-derivative Gaussian lineshape fit to the experimental data (after Ref. 27).

 © 2000 COSiW SEP, Warsaw

Table 2. The calculated transition energy values for 11H, 11L, 22H and bulk $Cd_{1-x}Mn_xTe$, made for undoped structure and those obtained from the experiment, for Sample 1 and Sample 2.

	Energy [eV]			
	11H	11L	22H	CdMnTe
From calculation	1.563	1.578	1.693	1.890
Sample 1 – from exp.	1.563	1.577	1.705	1.893
Sample 2 – from exp.	1.572	1.575	1.736	1.891

All of above discussed quantum structures were undoped. Using photoreflectance, it is also possible to investigate doped structures. The influence of indium planar doping on CdTe/$Cd_{1-x}Mn_xTe$ MQW structures was investigated by Sitarek *et al.* [28]. The samples used in that investigation were grown by MBE on GaAs substrates. The two studied heterostructures consisted of 50 periods of CdTe/$Cd_{1-x}Mn_xTe$ with thickness of 8 nm and 13 nm, respectively. The samples were planar doped with indium in the centre of the wells.

Room temperature PR spectra for the structures are shown in Fig. 9. The result for Sample 1 is shown in part (a) of the figure. Part (b) presents a spectrum for Sample 2, which had four times higher impurity concentration than Sample 1. Solid lines were obtained from a fit of the FDGL shape to the experimental data. Four oscillators were assumed for both spectra. Optical transitions, obtained from the fit, are marked in the figure as vertical lines. The transition energies are listed in Table 2. The optical transitions of undoped structure were calculated using the envelope function approximation. Calculated energies are also listed in Table 2.

The higher energy resonances originate from optical transitions in the CdMnTe layers. The Mn content estimated from the higher energy peaks position is 27%. The lower energy resonances were identified as 11H, 11L and 22H optical transitions.

For Sample 1 (with the lower In concentration) the energy values of 11H and 11L transitions obtained from the experiment agree very well with transition energies obtained from calculations. Only transition 22H is blue shifted by 12 meV compared to an undoped structure. For the second structure (with higher In concentration) there is relatively large blue shift of 11H and 22H transition energies and small red shift of 11L transition energy comparing to the transition energy values of undoped structure. The planar doping in the middle of the wells affects in some way the well potential. Doping has grater influence on the optical transition energies between heavy-hole subbands and electron subbands than on the transition energies between light-hole subbands and electron subbands.

As long as the barriers in multiple quantum wells structure is thick, coupling between the wells does not occur. The simplest structure containing coupled QWs is double quantum well (DQW). Sęk *et al.* [29] studied undoped symmetric structure with two GaAs/AlGaAs quantum wells separated by an AlAs mono-layer (ML). Structure was grown by the MBE on (001) semi-insulating GaAs wafer. In Fig. 10, a room temperature PR spectrum for the investigated structure is shown. Few resonances related to DQW transitions occur above the feature related to GaAs band gap transition. The transitions are labelled according to the common notation with indices s and a, where index s (a) means the transition between symmetric (antisymmetric) states. Sęk *et al.* obtained a very good agreement between the experimental transition energies and those from theoretical calculations based on envelope function approximation.

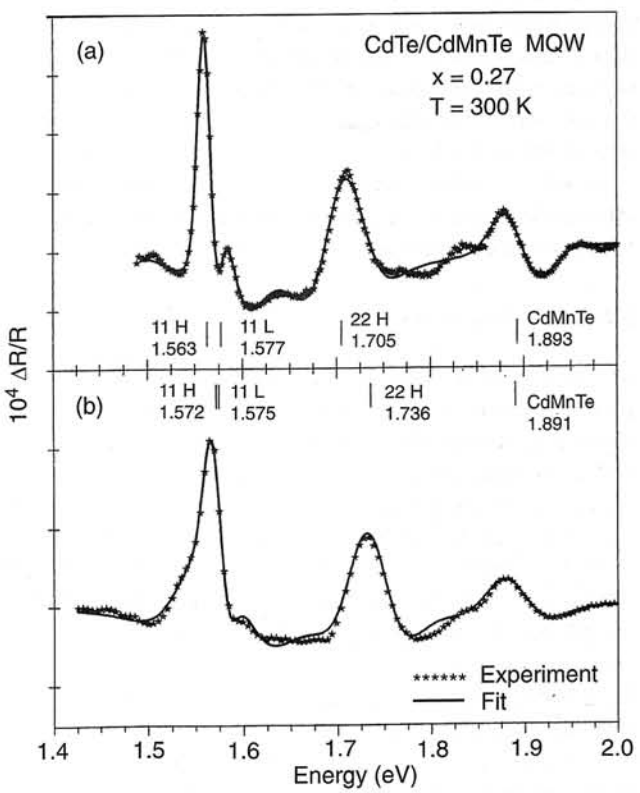

Fig. 9. Room temperature PR spectra of two CdTe/CdMnTe MQW structures with different dopand concentration. Solid lines are obtained from a fit to the experimental data with first-derivative Gaussian lineshape. Vertical lines marks the optical transition energies obtained from the fit (after Ref. 28).

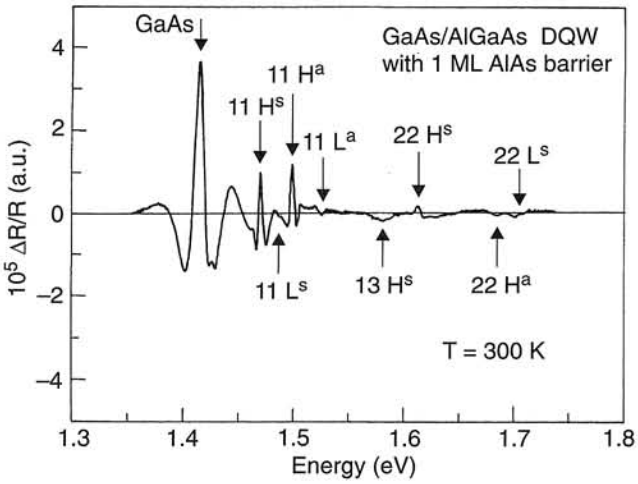

Fig. 10. Photoreflectance spectrum from the $GaAs/Al_{0.3}Ga_{0.7}As$ double quantum well structure. Arrows indicate the experimental transition energies (after Ref. 29).

Using PR spectroscopy, Labrie and Dubowski [30] reported an evidence of miniband dispersion in a CdTe/CdMnTe superlattice structure. The SL structure consisted of 49 periods of 5.4 nm thick CdTe wells and 2.7 nm thick $Cd_{0.9}Mn_{0.1}Te$ barrier layers. The structure was grown by the pulsed laser evaporation and epitaxy on a $Cd_{0.95}Zn_{0.05}Te$ substrate. Figure 11 shows the PR spectrum of the structure. The features observed in the 1.62–1.65 eV energy range are attributed to the fundamental QW transitions occurring at the Brillouin minizone centre (index "0"). The feature near 1.742 eV is attributed to the transition occurring in the CdMnTe layers. Two very weak resonances are observed at 1.679 eV and 1.695 eV. Labrie and Dubowski. attributed these two features to the $11H^1$ and $11L^1$ transitions, occurring at the edge of the mini Brillouin zone.

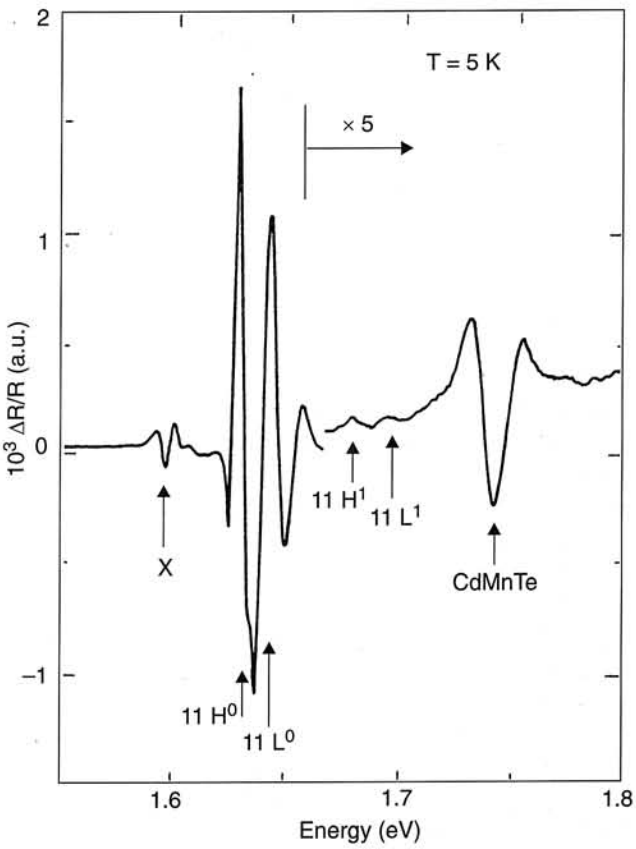

Fig. 11. Photoreflectance spectrum of $CdTe/Cd_{0.9}Mn_{0.1}Te$ superlattice taken at 5 K. Index '0' mark the transitions at the Brillouin minizone centre. Transitions occuring at the Brillouin minizone edge are marked with index '1'. The feature X is due to an excitonic-related transition occurring in the CdZnTe substrate (after Ref. 30).

3.2. Quantum wires

The first time the study of the optical properties of quantum wires, fabricated by electron beam lithography and reactive ion etching (RIE) in $SiCl_4$ were reported by Tang and co-workers [31].

The structure was grown by MBE technique. A 300 nm Si buffer layer, followed by a 50 nm $Si_{0.8}Ge_{0.2}$ layer (QW), a 30 nm undoped Si spacer and a 50 nm 5×10^{18} cm^{-3} boron doped Si layer were grown on a (100) silicon substrate. The sample was divided into several 5×5 mm chips. Using electron beam lithography followed by RIE, the chips were patterned with a series of 2.5 μm long and 10 nm to 500 nm wide wires.

The photoreflectance measurements were carried out at room temperature. The PR spectra of the quantum wires structures and a control structure are shown in Fig. 12. The arrows mark 11H optical transitions between the first heavy hole subband and the first electron subband. The 11H transition, in the case of control sample, originates from $Si_{0.8}Ge_{0.2}/Si$ quantum well. The reduction of the wire width to 200 nm did not change the energy associated with the 11H transition. The resonance, corresponding to 11H transition, in a 100-nm wide quantum wire is red shifted. Strain relaxation, produced during the wire fabrication, is responsible for the red shift of the resonance. The effect of dimension reduction is observed for quantum wires with width of 40 nm and less. When the width of wires decreases, the 11H transition energy shifts to higher energies. A quasi one-dimensional (1D) confinement in the system and a strain relaxation process arising from the dry etching determine the 11H transition energies in these wires.

3.3. Quantum dots

With nanoscale lithographic techniques used to 2D heterostructures, it is possible to obtain quantum dots (QD), quasi zero dimensional (0D) objects.

Qiang and co-workers [32] reported room temperature PR studies of $GaAs/Ga_{0.7}Al_{0.3}As$ quantum dots arrays, fabricated by reactive ion etching. An MBE structure consisting of a 500 nm of a not intentionally doped GaAs buffer layer followed by 100 periods of GaAs (8 nm)/$Ga_{0.7}Al_{0.3}As$ (12 nm) quantum wells, capped by 10 nm of GaAs, was

 © 2000 COSiW SEP, Warsaw

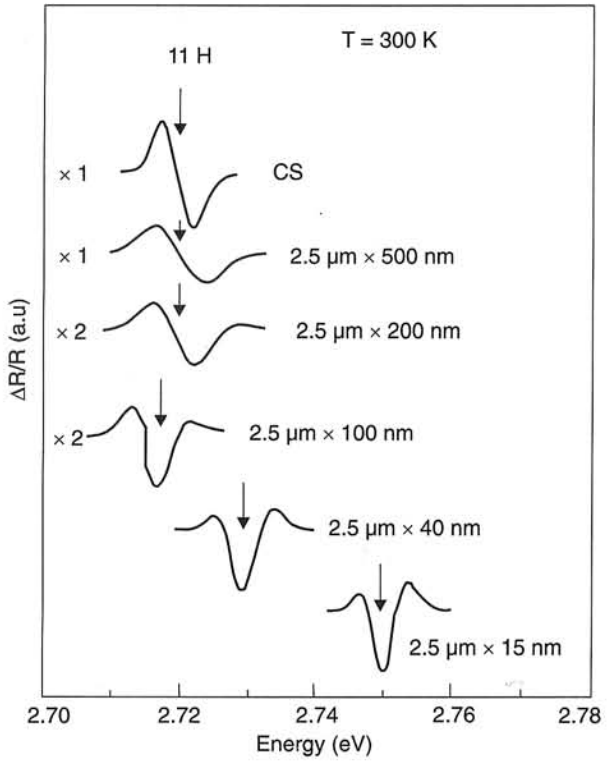

Fig. 12. Photoreflectance spectra of $Si_{0.8}Ge_{0.2}$/Si quantum wires of different width and the spectrum of the control structure (CS) (after Ref. 31).

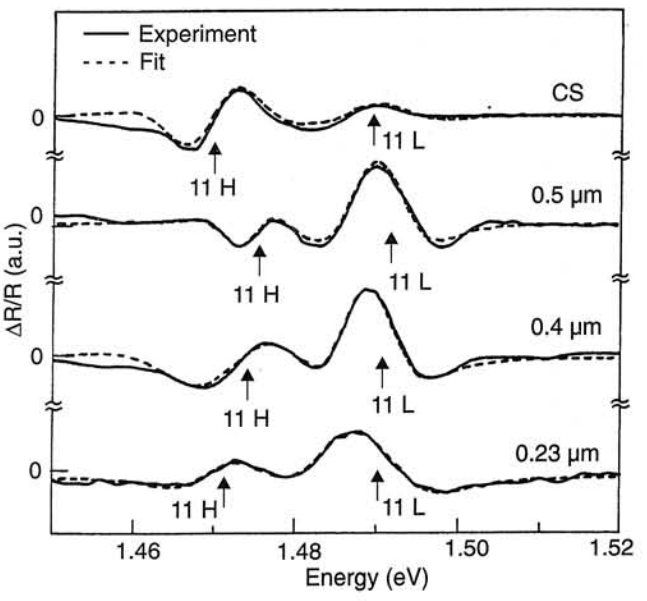

Fig. 13. Photoreflectance spectra at 300 K in the region of 11H and 11L transitions from three GaAs/$Al_{0.3}Ga_{0.7}$As quantum dot arrays and a spectrum of the control structure (after Ref. 32).

grown on (001) semiinsulating GaAs substrate. Three quantum dot arrays, with lateral size of 500 nm, 400 nm and 230 nm, and MQW control structure have been investigated. The distance between the dots was four times greater than their diameter.

The solid lines in Fig. 13 show room temperature photoreflectance spectra of the control sample and the QD arrays. The dashed lines are the least-squares fits of the data to the first derivative of a Gaussian profile. The calculations yield the energy positions and the broadening parameters of PR features. Obtained from the experiment energies of 11H and 11L optical transitions are denoted in Fig. 13 by arrows.

The energy positions of 11H and 11L from the control sample are consistent with an 8 nm GaAs quantum well. The energy of the 11L transition varies very little from sample to sample. When compared to the control sample, the energy of 11H optical transition in the 500 nm dot structure is blue shifted by about 5 meV. It decreases to almost its original position (in the control sample) in 230 nm dot array. The strain induced by the RIE is fairly uniform resulting in small differences in the broadening parameters for all resonances.

Qiang *et al.* explained the behaviour of 11H and 11L transition energies in terms of the strains in the quantum dots. For the 500 nm dots there is a compressive strain of about -7×10^{-4} along the growth direction. Reduction in strain was observed when the lateral dimension of QD decreases. For the structure with smallest dots the strain has been reduced to about -2×10^{-4}.

Gumbs *et al.* [33,34] investigated the intersubband transitions from modulation-doped GaAs/GaAlAs quantum dot arrays fabricated by RIE. By using PR performed at 77 K and 300 K, they studied two quantum dots structures with dots of 60 nm and 100 nm in diameter.

Klar *et al.* [35] investigated high-density patterns of ZnTe/$Zn_{0.93}Mn_{0.07}$Te quantum dots. Quantum dots with a diameter of 200 nm were prepared by electron lithography followed by Ar^+ ion beam etching from four MBE grown ZnTe/$Zn_{0.93}Mn_{0.07}$Te MQW structures with 4 nm, 6 nm, 8 nm and 10 nm well widths. Photoreflectance measurements were performed at 10 K. The modulation was carried out with a 632.8 nm (1.96 eV) He-Ne laser (below-bandgap photomodulation). Klar *et al.* showed that the main effect of the nanofabrication process is a change in the strain of the quantum dot structures when compared with control sample. Parent structure is in a good approximation strained to the ZnTe buffer layer whereas quantum dots are unstrained.

For light hole excitons, an increase in the oscillator strength was observed in the QD structures. An electric dipole moment, parallel to the growth direction, introduced by the probe light that can penetrate the QD side walls (the side walls are not perpendicular to the surface) is a possible explanation of this effect.

Klar and co-workers did not observed any confinement effects due to the reduction of the dimensionality from 2D to 0D. The lateral sizes of dots being under study were too large to observe such confinement effects.

Quantum dot structures, described in above papers, were obtained by the lithography followed by etching pro-

cesses. The size of dots and the level of perfection in such structures are limited by the lithographic processing. Using an epitaxial growth of materials with a large lattice mismatch is a way of obtaining islands of small lateral size of one material grown on the other material. Quantum dots obtained in such a way are referred as "self-assembled" or "self-organised".

Ulrich *et al.* [36] used the above method to obtain nanoscale InP islands embedded in $In_{0.48}Ga_{0.52}P$ matrixes. The structures were grown by MBE on (001) GaAs substrate. The substrate layer was followed by 200 nm of $In_{0.48}Ga_{0.52}P$ and three to ten monolayers of InP, covered by another 200 nm $In_{0.48}Ga_{0.52}P$ cap layer. The atomic force microscope (AFM) pictures showed that the island density is of the order of 10^{10} cm^{-2}. This structure, with nominally three monolayers of InP, formed dots (islands) of 20–30 nm in diameter and a 5–10 nm high. When a number of monolayers increase to seven monolayers, the dot diameter increases up to 40–50 nm.

Figure14 presents photoreflectance spectra, measured at 300 K, for structures with three and seven monolayers of InP, respectively. Both spectra show resonances corresponding to E_0(GaAs), $E_0 + \Delta_0$(GaAs) and E_0(InGaP) optical transitions. The transition denoted as 11H is an optical transition between the first heavy hole and the electron states of the InP islands. For the three-monolayer sample, the 11H transition is partially obstructed by the PR feature of $E_0 + \Delta_0$(GaAs) transition. The transition labelled 22H is observed in the PR spectrum of the seven-monolayer sample. Ulrich *et al.* proposed a simple, based on the envelope-function approximation, theoretical model to calculate the subband energies. The transition energies, obtained from the theoretical considerations, agree well with energy values obtained from experiment for the structures with InP nominal thickness between three and ten monolayers.

Sęk *et al.* used room temperature photoreflectance spectroscopy to investigate optical transitions in MOCVD--grown, InAs/GaAs structures with self-organised quantum dots [37]. Tellurium doped GaAs substrate was followed by 100 nm GaAs buffer layer, 25 nm of $Al_{0.3}Ga_{0.7}As$, 100 nm of GaAs and 1.65 monolayer of InAs. A strong lattice mismatch between the latter two compounds induces a formation of InAs pyramids. The QD pyramids are covered by 1 nm of $In_{0.3}Ga_{0.7}As$. This structure was then covered with 20 nm of GaAs, 25 nm of $Al_{0.3}Ga_{0.7}As$ and capped with 20 nm of GaAs. From the transmission electron microscope measurements, the diameter of the dots is in 10–12 nm range while the height is about 2.5–3 nm.

A room temperature PR spectrum of the investigated QD structure is presented in Fig. 15 (circles). In the figure, we can see three groups of features related to quantum dots, InAs wetting layer and GaAs band gap, respectively. The features labelled QD1, QD2 and QD3 correspond to optical transitions in quantum dots. The resonances designated as WL1 and WL2 correspond to the 11H and 11L transitions in the step-shaped quantum well, formed in the InAs wetting layer and the $In_{0.3}Ga_{0.7}As$ layer covering the dots.

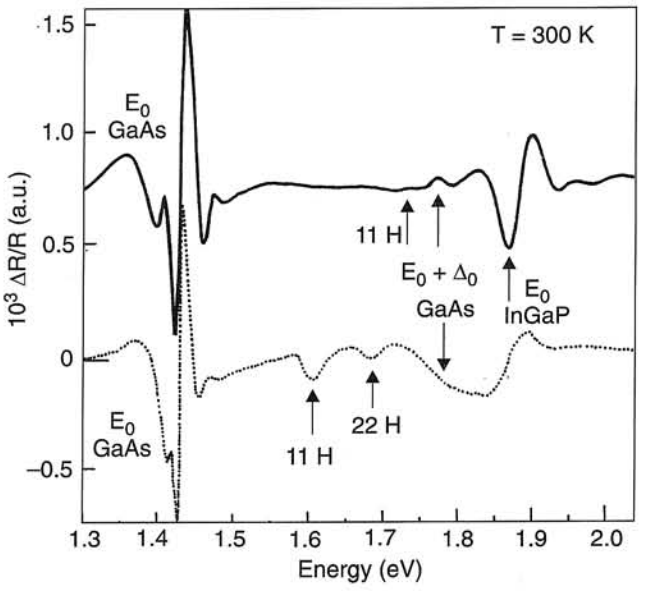

Fig. 14. Photoreflectance spectra of $InP/In_{0.48}Ga_{0.52}P$ island (dot) structures with 3 ML (solid line) and 7 ML (dashed line) of nominal InP thickness (after Ref. 36).

In order to obtain the transition energy values, fitting of the first derivative of a Gaussian line shape to the experimental data was performed. The FDGL fit is presented in Fig. 15 as the solid line. The interpretation of QD related transitions was possible after theoretical calculations for buried, pyramid shaped InAs QD's on (001) GaAs bound to {101} facets. Assuming a pyramidal shape of the dots, accounting for strain distribution, piezoelectricity, valence band mixing and conduction-band valence-band coupling, the electronic structure and optical properties were modelled using 8-band **k·p** theory. After extrapolating these results to room temperature and taking into account the

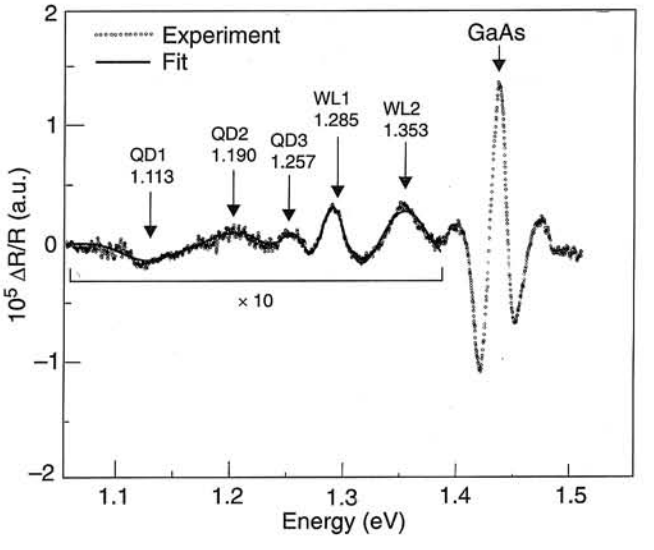

Fig. 15. Room temperature PR spectrum of InAs/GaAs quantum dot structure (circles). Solid line represents a fit according to the first-derivative Gaussian lineshape to the experimental data. Arrows indicate the transition energies (after Ref. 37).

 © 2000 COSiW SEP, Warsaw

exciton binding energy, the obtained transition energy values are in good agreement with the experimental results. QD1, QD2 and QD3 transitions were identified as e0-h0, e2-h1 and e1-h3, respectively, where e0 (h0) denotes the ground electron (hole) state.

Rowland and co-workers [38] presented photoreflectance spectra of MBE grown, self-assembled InAs/GaAs quantum dot structures.

4. PR study of semiconductor devices

In the previous section, it was shown that photoreflectance spectroscopy is a powerful tool for investigation of characteristic properties of low dimensional semiconductor heterostructures, like quantum well structures, quantum wires and quantum dots. The PR technique may be used not only for characterisation of the low-dimensional structures but for the investigation of semiconductor devices structures as well. In the next few paragraphs, we will present applications of PR spectroscopy for studies of a high electron mobility transistor (HEMT) structure, a pseudomorphic HEMT (PHEMT) device, a heterojunction bipolar transistor (HBT), and a vertical/planar light emitting laser.

4.1. Transistors

4.1.1. High electron mobility transistors

A HEMT structure is formed by a charge transfer from a heavily doped AlGaAs layer to an undoped GaAs layer. This process places the electrons in a very pure GaAs layer, resulting in very high electron mobility. Figure 16 shows a schematic of such structure. The electrons transferred to the GaAs layer are confined to the interfacial region and form a two-dimensional electron gas (2DEG) in a nearly triangular potential well. In order to avoid Coulomb interactions between the electrons with enhanced electron mobility in

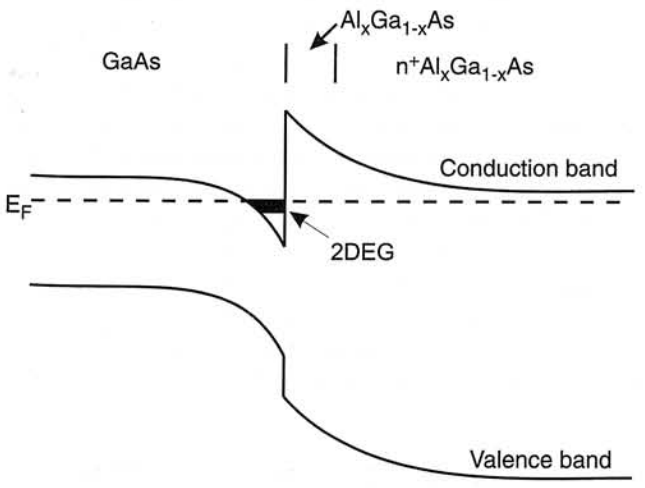

Fig. 16. Schematic diagram of a HEMT structure.

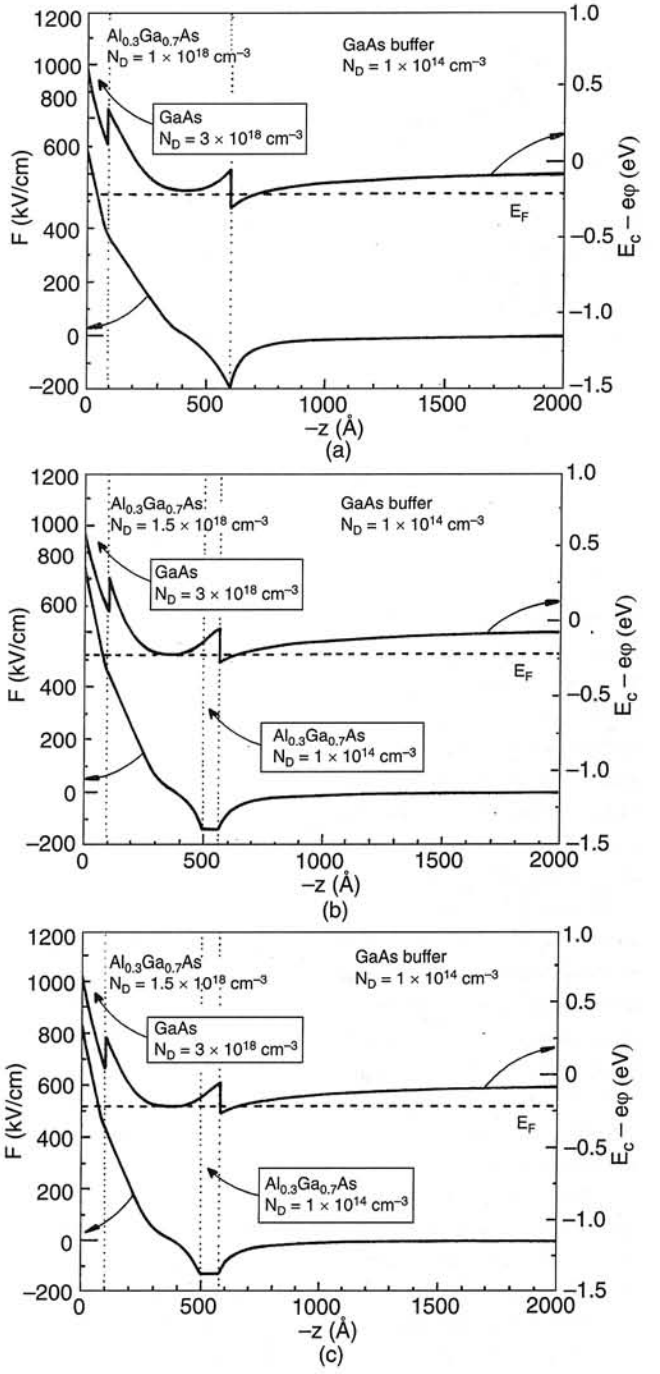

Fig. 17. Electric potential and field profiles for AlGaAs/GaAs HEMT structures 1 (a), 2 (b) and 3 (c) (after Ref. 39).

2DEG and the ionised donors in n^+ AlGaAs layer, an insulating AlGaAs spacer layer usually separates these two layers. The thickness of spacer determines the number of transferred electrons. The presence of a potential well results in the formation of subband states in the conduction band. The valence band exhibits no confinement and hence has three-dimensional characteristics.

Soares and co-workers [39,40] investigated three AlGaAs/GaAs HEMT structures with different spacer width. All structures were grown by MBE on a semi-insulating GaAs substrate. The GaAs substrate was followed by

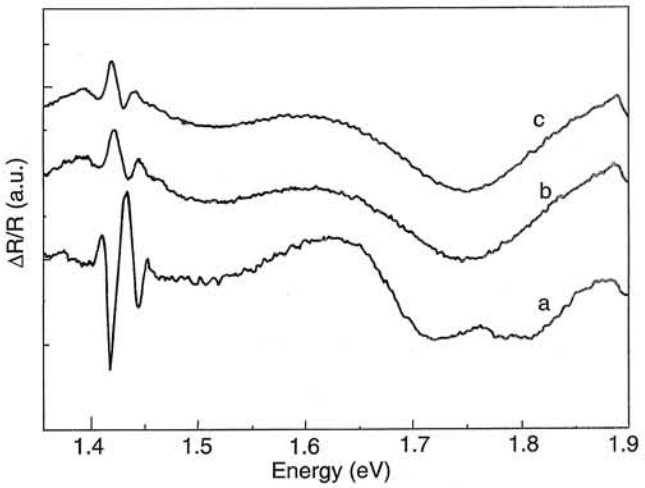

Fig. 18. Photoreflectance spectra from AlGaAs/GaAs HEMT structures 1 (a), 2 (b) and 3 (c) (after Ref. 39).

500 nm undoped active GaAs layer, an undoped $Al_{0.3}Ga_{0.7}As$ spacer, an Si-doped $Al_{0.3}Ga_{0.7}As$ barrier layer and an Si-doped GaAs cap layer of donor concentration $N_D = 3\times10^{18}$ cm^{-3}. The width and donor concentrations of the barrier layers were 50 nm and $N_D = 1\times10^{18}$ cm^{-3} for structure 1 and 40 nm and $N_D = 1.5\times10^{18}$ cm^{-3} for structures 2 and 3, respectively. The thickness of the spacer layer was 0 nm, 6 nm and 8 nm. The potential and electric field profiles of the HEMT structures are shown in Fig. 17.

Figure 18 presents room temperature PR spectra of the three HEMT structures. Each spectrum exhibits two types of oscillations: short-period oscillations at the fundamental gap of GaAs and extending over the whole spectral range, wide-period oscillations. The wide-period oscillations originate from the Franz-Keldysh effect. The strength of surface electric field, obtained from the period of FKO, is slightly less than that obtained from electric field profile calculations (about 750 kV/cm).

The short-period oscillations in structure 1 differ from oscillations in the other structures. For example, the amplitude of these oscillations is considerably smaller for structures 2 and 3 than for structure 1. The deviations, between structure 1 and the other structures, concerning GaAs layers occur only at the AlGaAs/GaAs interfaces. Thus, Soares *et al.* attributed the line shape discrepancies to different interface qualities. In the case of sample 1, the interface is of relatively good quality and the charge density, associated with the interface defects, is small. Interface defects and the associated interface charge seem to be present in the case of samples 2 and 3. The quality of interface influences the electric field profile and hence the PR spectra. The short-period oscillations cannot be traced back to the Franz-Keldysh effect. Soares *et al.* assumed that the origin of these features is from optical transitions to subband states above the Fermi level. These subbands are formed in AlGaAs/GaAs potential well.

Glembocki and co-workers [1] have shown that the PR technique provides a room temperature fingerprint of

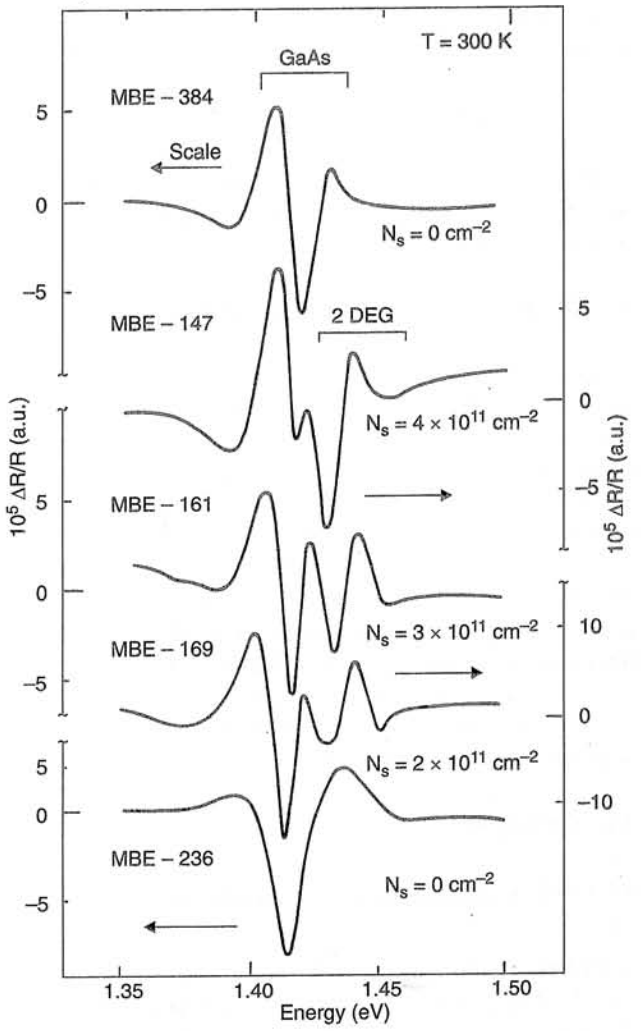

Fig. 19. Photoreflectance spectra of an undoped AlGaAs/ GaAs heterojunction (top) and four HEMT structures with different carrier densities (after Ref. 1).

a two-dimensional electron gas. They have studied a few of HEMT structures with different electron gas concentration. Figure 19 shows a series of spectra ranging from thick layers to a HEMT structure, which failed to form the two-dimensional electron gas. Only one feature, which originate from the GaAs layer, is present in the spectrum of the structure without the two-dimensional electron gas (the top spectrum). The two-dimensional carrier concentration was measured with a cyclotron resonance technique at 4 K. Formation of a two-dimensional electron gas results in an additional PR feature above the GaAs sigal. The intensity of this feature decreases as the carrier density is reduced, until it is hardly visible in the structure having zero carrier density at 4 K. Low temperature measurements indicates that this feature does not originate from the Franz-Keldysh effect. Although the nature of the PR feature is still unknown [1], it serves as a fingerprint of a two-dimensional electron gas.

Sęk *et al.* [41] studied two AlGaAs/GaAs HEMT structures grown by MBE. A buffer layer, 100 periods of

 © 2000 COSiW SEP, Warsaw

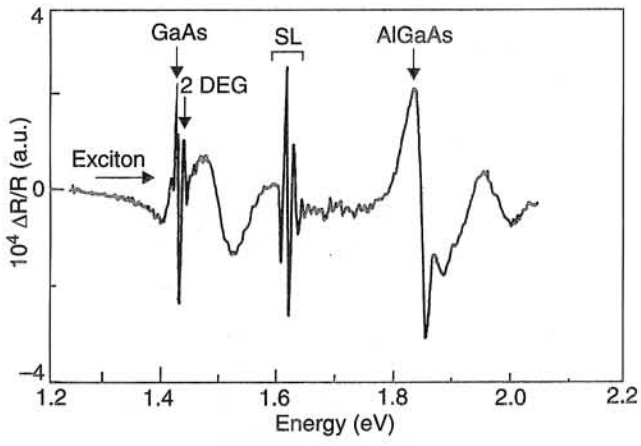

Fig. 20. Room temperature spectrum from $Al_{0.33}Ga_{0.67}As$/GaAs HEMT structure (after Ref. 41).

GaAs(2.5 nm)/AlGaAs(2.5 nm) superlattice, 510 nm GaAs active layer, AlGaAs spacer layer of 40 or 80 nm width and 200 nm n-doped (1×10^{17} cm^{-3}) AlGaAs layer were grown on a GaAs substrate. The structure was terminated with a 17 nm GaAs cap layer.

A PR spectrum of HEMT structure with an 80 nm spacer layer, is presented in Fig. 20. The spectrum can be divided into several independent regions. In the region around 1.42 eV, the main peak corresponds to GaAs band gap transition. A weak peak, visible in the low--energy part of this spectrum, is related to the excitonic transition. The additional resonance at 1.435 eV is probably related to a two-dimensional electron gas. Sęk *et al.* interpreted the oscillatory signal around 1.6 eV, as the Franz-Keldysh oscillations associated with the SL present in the structure. In the presence of an internal electric field, the electrons can be accelerated in the field direction and transitions in short-period SL may be analysed in terms of the miniband Franz--Keldysh effect. The electric field value, deduced from the period of the oscillations, is 4.4 kV/cm.

Between 1.45 eV and 1.6 eV there is a broad oscillation. Such an oscillation is characteristic for the Franz--Keldysh effect from the fully depleted GaAs cap layer. A feature, corresponding to the AlGaAs band gap transition, appears in the spectrum above 1.85 eV. From the position of this resonance, the Al content was deduced to be 33%. An additional feature is present at about 1.95 eV. This feature probably results from to the overlapping of two Franz-Keldysh oscillations associated with AlGaAs band gap resonances from different parts of structure: from the highly doped AlGaAs layer and the undoped AlGaAs spacer.

Photoreflectance spectrum obtained from the structure with a 40 nm spacer layer was very similar to the previous one. The only difference was in the absence of the excitonic feature due to the higher (6.3 kV/cm) electric field formed in this structure.

4.1.2. Pseudomorphic high electron mobility transistors

High electron mobility transistors offer superior signal-to--noise performance compared with other solid state amplifiers. One type of HEMT, the pseudomorphic AlGaAs/InGaAs/GaAs modulation doped structure (PHEMT) has demonstrated outstanding power performance. The pseudomorphic structures overcome the problem associated with the DX centres in the AlGaAs in AlGaAs/GaAs HEMTs, and make it possible to achieve a larger conduction band discontinuity for a given Al content. In the AlGaAs/InGaAs/GaAs system, large electron concentration in the two-dimensional gas can be achieved while the electron mobility remains very high. These structures promise device performance up to few hundred GHz. The energy band profile of PHEMT structure is shown in Fig. 21.

A detailed study of a pseudomorphic $Al_{0.22}Ga_{0.78}As$/$In_{0.21}Ga_{0.79}As$/GaAs HEMT structure in the temperature range from liquid nitrogen to the room temperature was reported by Yin *et al.* [42]. The structure was fabricated with MBE on (001) GaAs substrate. It has similar profiles as those in HEMTs used for both low-noise and power amplification at 94 GHz. A 300 nm of not-intentionally doped GaAs, followed by 15 nm of $In_{0.21}Ga_{0.79}As$, 3 nm of $Al_{0.22}Ga_{0.78}As$, a planar Si doping layer of 5×10^{12} cm^{-2}, 50 nm of $Al_{0.22}Ga_{0.78}As$ and a 5 nm GaAs cap, was grown on top of buffer structure. From Hall measurements, sheet electron densities of $N_s = 2.3\times10^{12}$ cm^{-2} at 77 K and $N_s = 2.5\times10^{12}$ cm^{-2} at 300 K were determined.

Figure 22 shows both the PR and the electroreflectance (ER) spectra of PHEMT structure. Features below 1.4 eV, labelled A, B and C, are associated with InGaAs quantum well. Features between 1.4 eV and 1.45 eV originate from GaAs and features at about 1.75 eV from the AlGaAs layer. Peaks at low energies, comparing to these from AlGaAs,

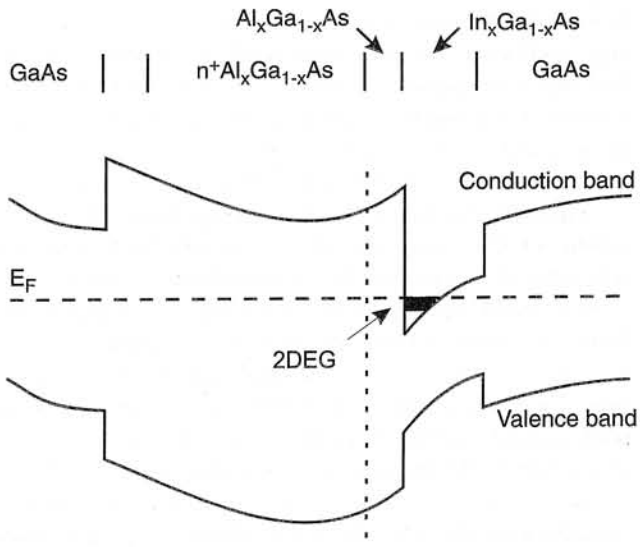

Fig. 21. The energy band profile of PHEMT structure.

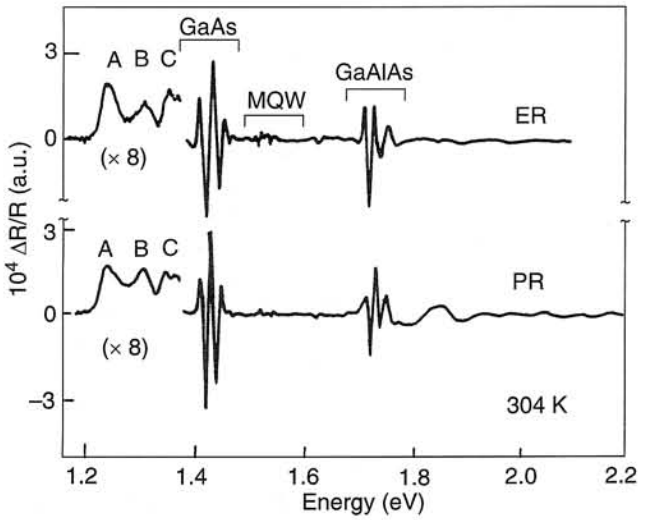

Fig. 22. Photoreflectance and electroreflectance spectra from AlGaAs/InGaAs/GaAs PHEMT structure. Features labeled A, B and C are associated with InGaAs quantum well (after Ref. 42).

originate from GaAs/AlGaAs MQW. The part of the spectrum originating from InGaAs quantum well is the most interesting. Line shapes of A, B and C features are unusual for modulation spectroscopy from QW system. The traces should have positive and negative lobs but in this case they lie on only one side of the baseline. Also, the peak labelled as A is asymmetric on the high-energy side. This asymmetry property is due to the Fermi level filling factor. This enabled Yin *et al.* to determine the Fermi energy and hence N_s.

In order to identify the origins of the A, B, and C peaks, Yin and co-workers performed a self-consistent theoretical calculation. They found very good agreement between ER experiment and theory associating features A, B and C with 21H, 32H and 42H transitions, respectively. Transitions, which involve the ground electron subband, are not allowed since E_F lies above this level. The densities of two-dimensional electron gas, obtained from the data, are in a good agreement with the Hall results. The Fermi energy (and hence N_s), obtained from the PR studies, is larger than that corresponding to the ER measurements. The discrepancy results from the presence of carriers photoexcited by the pump beam. Decreasing the pump light intensity can reduce the differences between the PR and ER spectra.

Yin *et al.* also performed room temperature PR investigations of three different AlGaAs/InGaAs/GaAs PHEMT structures [43]. Besides the investigations of InGaAs region of the PR spectra, they studied features related to the GaAs and AlGaAs layers. They deduced corresponding to the GaAs and AlGaAs electric fields and the Al composition. The field related to the GaAs signal is in agreement with a calculated built-in electric field. The Al composition also confirms the intended growth conditions.

Han and co-workers studied the AlGaAs/InGaAs/AlGaAs PHEMT structures with different doping profiles [44]. The doping on both sides of the InGaAs channel affects the electric field in GaAs and AlGaAs layers. The front side doping (Si delta doped top AlGaAs layer, 2 nm from AlGaAs/InGaAs interface) has more influence on the Franz-Keldysh oscillations (electric field) in the AlGaAs layer. Back-side doping (Si doped AlGaAs layer 3 nm below InGaAs/AlGaAs interface) has more effect on the Franz-Keldysh oscillations of the buffer GaAs feature. Han et al. has not found any relationship between the electric field present in the structure and the channel carrier concentration.

Using photoreflectance, Liu et al. has studied the behaviour of a two-dimensional electron gas in PHEMT structures [45]. The samples were grown by MBE. The energy band profile of the AlGaAs/InGaAs/GaAs PHEMT structure being under study is shown in Fig. 21. The InGaAs channel has a thickness of 15 nm. Both aluminum and indium mole fraction was 15%. The AlGaAs spacer layer is 3 nm thick, while the n-type doped AlGaAs layer has thickness of 30 nm. The structure was covered by 15 nm of n-type doped GaAs. From Hall measurements, a two-dimensional electron gas density of 1.2×10^{12} cm^{-2} was obtained. Figure 23 shows the spectra obtained at temperatures from 20 to 300 K. The low energy side of the spectra are related to the two-dimensional electron gas in the InGaAs channel. The features from InGaAs channel are

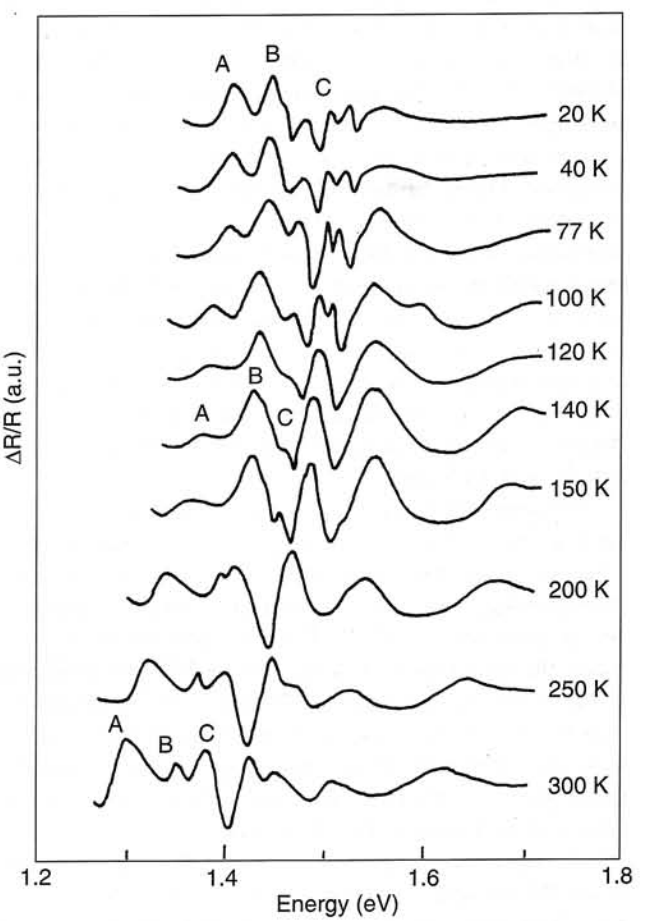

Fig. 23. The photoreflectance spectra of AlGaAs/InGaAs/ GaAs PHEMT structure at various temperatures. The features from InGaAs channel are denoted as A, B and C (after Ref. 45).

 © 2000 COSiW SEP, Warsaw

denoted as A, B and C. At 300 K, feature C is superimposed with the signal from the band edge signal of GaAs. Feature C becomes separated at 20 K and displaying derivative-like characteristics. Calculation based on triangular well potential, shows that this feature is related to the 22H optical transition. The derivative-like behaviour implicates that the band filling effects and screening effects are not important for 22H transition. Features A and B are related to the 11H and 12H transitions, respectively. Due to the presence of the two-dimensional electron gas and consequently, the band filling and screening effects, these transitions are weakened and their line shapes keep asymmetric at various temperatures. At both low and high temperatures, the influence of the band filling has different effects, which results in the absorption onset near the bottom of ground states at room temperature and near the Fermi edge at low temperatures, respectively.

4.1.3. Heterojunction bipolar transistors

There is a considerable interest in heterojunction bipolar transistor (HBT) technology for a use in high-speed digital circuits and efficient microwave devices. The large valence band discontinuity at the emitter-base junction introduces an energy barrier, which limits the injection of minority carriers from the base to the emitter. Hence, the emitter injection efficiency and the current gain can be improved significantly. An important drawback of HBT is a large collector-emitter offset voltage resulting from the turn-on voltage difference between the emitter-base heterojunction and base-collector homojunction.

Bottka *et al.* [46] has studied AlGaAs/GaAs HBT structures grown by MOVPE technique. The layer parameters of the structures are given in Table 3. After growth, HBTs were fabricated in a portion of the wafer. In order to assess transistor performance, current-voltage (I-V) and capacitance-voltage (C-V) characteristics were collected. Sample A exhibits good current gain ($\beta = 50$) and a high collector-emitter breakdown voltage (greater than 18 V). Sample B was grown on a thick base layer and, due to the bulk recombination, exhibits lower current gain ($\beta = 5$). Sample C was prepared multiple times and demonstrated reasonable or no current gain (poor emitter injection efficiency), depending on the growth conditions employed.

Figure 24 shows PR spectra from sample B, obtained using 400 Hz modulated 488 and 633 nm laser light. In part (a) of the figure, the damped oscillations between 1.45 and 1.7 eV correspond to Franz-Keldysh oscillations mainly from the emitter-base space charge region. An electric field corresponding to these oscillations is about 130 kV/cm. In part (b) of the figure, an additional lower period Franz-Keldysh oscillation is observed in the spectral region between 1.44 and 1.5 eV. This feature originates from the base-collector space charge region. The oscillatory structure above 1.79 eV corresponds to the Franz-Keldysh oscillations of the $Al_xGa_{1-x}As$ emitter layer, having an electric

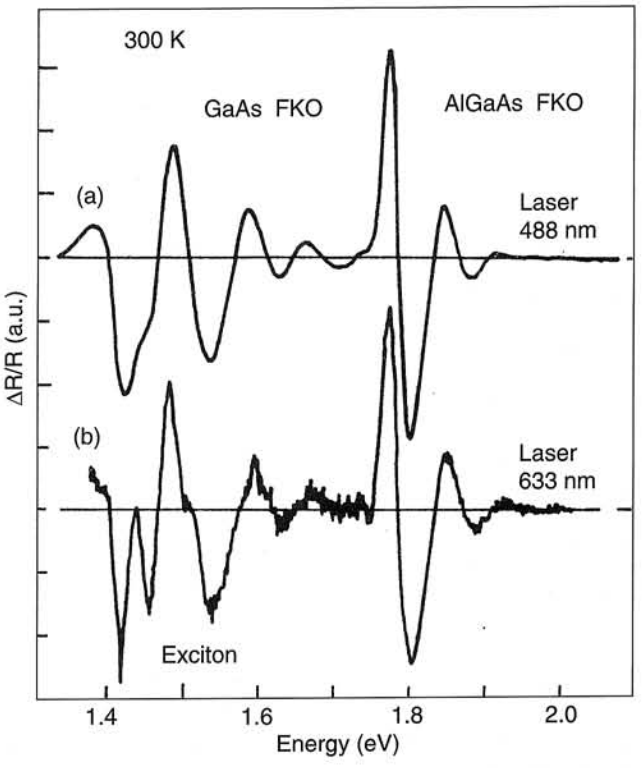

Fig. 24. Room temperature photoreflectance spectra from wide base AlGaAs/GaAs HBT structure – sample B (after Ref. 46).

field of about 100 kV/cm. The x = 0.28 Al mole fraction, was deduced from the energy gap.

The base-emitter region is most critical for the overall device performance. Small difference in the placement of the base-emitter p-n junction can have considerable impact on the device. From the analysis of certain spectral features, Bottka *et al.* has evaluated the built-in DC electric field in both the AlGaAs emitter and in the n^- GaAs collector region.

Sun and Pollak [47] studied the origin of the Franz-Keldysh oscillations, observed in photoreflectance spectra, associated with the electric fields in the AlGaAs emitter and the GaAs collector of graded band gap heterojunction bipolar transistors. They derived analytical expressions for the origins of the Franz-Keldysh oscillations, associated with the fields in the graded emitter and collector regions of AlGaAs/GaAs HBT. Sun and Pollak found that the oscillations from the collector are a measure of the maximum collector space charge field at the collector-base junction. The Franz-Keldysh oscillations, originated from the graded band gap AlGaAs emitter, are a function of both the space charge field and emitter-base grading dimension.

Compared to GaAs/AlGaAs based structures, lattice matched $InP/In_{0.53}Ga_{0.47}As$ HBT structures have several advantages. Low turn-on voltage, low surface recombination rate and a use of the some substrates as sources and detectors of 1.3–1.55 μm wavelength radiation (favoured in optoelectronics) are some of the examples.

Table 3. The layer parameters for three AlGaAs/GaAs HBT structures – A, B and C (after Ref. 46).

Device layer	Al mole fraction	Sample A		Sample B		Sample C	
		Doping (cm^{-3})	Thickness (nm)	Doping (cm^{-3})	Thickness (nm)	Doping (cm^{-3})	Thickness (nm)
n^+ cap	0	5×10^{18}	200	5×10^{18}	100	4×10^{18}	200
N graded	0–0.3	2×10^{17}	30	2×10^{17}	30	1×10^{17}	20
N emitter	0.3	2×10^{17}	150	2×10^{17}	150	1×10^{17}	150
N graded	0.3–0	2×10^{17}	20	2×10^{17}	30	1×10^{17}	20
p^- spacer	0	1×10^{15}	20	1×10^{15}	20	1×10^{15}	20
p^+ base	0	1×10^{19}	100	1×10^{19}	500	1×10^{19}	80
n^- collector	0	3×10^{16}	700	1×10^{16}	500	4×10^{16}	500
n^+ sub-collector	0	5×10^{18}	500	5×10^{18}	500	4×10^{18}	300
Substrate	0	SI		SI		SI	

Using PR, Yan *et al.* [48] has investigated a grown by gas-source MBE, lattice-matched $InP/In_{0.53}Ga_{0.47}As$ HBT structure. They performed a room temperature measurement. From the periods of Franz-Keldysh oscillations, they evaluated both the built-in electric field to be 30 kV/cm and 100 kV/cm and corresponding donor levels of 4.5×10^{15} and 3.5×10^{16} cm^{-3} in n-InGaAs collector and n-InP emitter regions, respectively. The optical transition energy of InGaAs, indicates that this material is lattice matched to the InP.

A heterojunction bipolar transistor, based on InAlAs/InGaAs, has a lower break-down voltage than the two types of HBTs described above. Because of this fact, the InAlAs/InGaAs HBTs become an interesting topic in low-bias integrated-circuit applications. The simplest way to reduce the offset voltage is the method of inserting an intrinsic spacer, made of material with a small band gap, between the emitter and the base. Confining the two-dimensional electron gas, the spacer reduces the energy spike in the emitter-base junction.

Using photoreflectance spectroscopy, Hsu and Chen *et al.* have studied lattice-matched InAlAs/InGaAs HBTs, grown by MBE [49–52]. The structures were fabricated on an n^+ InP:Si substrate (001). The layer structure of the HBT samples is shown in Table 4. Two samples, with 30 nm and 50 nm width of the undoped InGaAs spacer layer, have been studied. Figure 25 shows a self-consistent calculated energy band diagram of sample with the 30 nm spacer layer.

Photoreflectance spectra of the studied structures are presented in Fig. 26. Spectrum #1 comes from the structure with the 30 nm spacer and spectrum #2 is for the structure with the 50 nm spacer. Features labelled as A and E denote the transitions due to the $In_xGa_{1-x}As$ band gap and the $In_yAl_{1-y}As$ band gap, respectively. From the energy position of these two features, In content x = 0.516 and y = 0.540 was obtained. The quantum confined excitonic transitions, with excitons formed by electrons confined to the QW in the emitter-spacer junction and unconfined holes in the valence band, are denoted as B. The features denoted C are due to the electronic transitions between the valence band and a subband edge in the triangular quantum well in the spacer portion. The $E_0 + \Delta_0$ transitions in InGaAs are labelled as D. The Franz-Keldysh oscillations near C and E are related to the built-in dc electric field. From the oscillations, Hsu *et al.* found, that the electric field in the InGaAs spacer and InAlAs emitter regions are 50.2 kV/cm and 107.6 kV/cm, respectively, for sample with L_S = 30 nm and

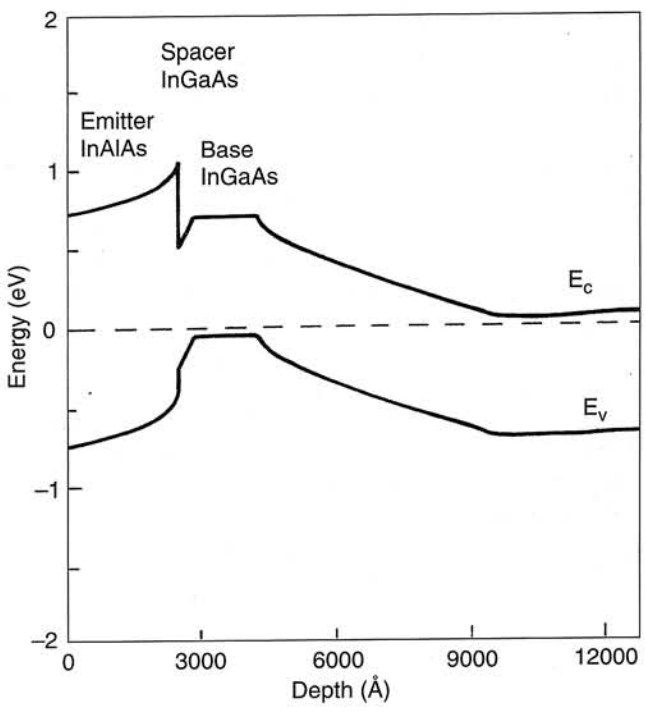

Fig. 25. Self-consistent calculated energy band diagram of InAlAs/InGaAs HBT with spacer layer of 30 nm (after Ref. 50).

 © 2000 COSiW SEP, Warsaw

Table 4. Layer structure of InAlAs/InGaAs HBTs. L_S is the width of spacer layer.

	Thickness (nm)	Doping (cm^{-3})
n^+ – InAs cap	30	3×10^{19}
n^+ – InGaAs cap	50	3×10^{19}
n – InAlAs Hi-emitter	100	2×10^{19}
n^+ – InAlAs emitter	150	1×10^{17}
i – InGaAs spacer	L_S	
p – InGaAs base	150	4×10^{18}
n – InGaAs collector	500	1×10^{15}
n – InGaAs Hi-collector	250	1×10^{17}
n^+ – InGaAs buffer	250	3×10^{19}
n^+ – InP substrate		

41.4 kV/cm and 107.6 kV/cm for sample with L_S = 50 nm. The electric field associated with C decreases as the spacer thickness increases. Hsu *et al.* estimated that the interface charge carrier density, N_S, is 3.54×10^{11} cm^{-2} for L_S = 30 nm and 4.22×10^{11} cm^{-2} for L_S = 50 nm.

Photoreflectance studies on the InAlAs/InGaAs HBT structure with L_S = 30 nm were continued by Chen and Jan [51]. They analysed the behaviour of a two-dimensional electron gas at temperatures between 10 K and 300 K. For the first time, Chen and Jan utilised the temperature dependence of effective mass to analyse Franz-Keldysh oscillations in the photoreflectance technique. The values deduced from the oscillations were in reasonable agreement with the based on intended growth condition calculations.

Chen and co-workers [53] investigated graded InAlAs/InGaAs HBT structures at temperatures between 8 K and 300 K. Using the Varshni and Bose-Einstein equations, they described the temperature variation of energy gaps. From the observed Franz-Keldysh oscillations, they evaluated the built-in electric fields in the i-InGaAs collector, i-InGaAs spacer and n-InAlAs emitter regions. In the interfaces between emitter and base, the electric field values are in good agreement with the continuity condition of electric displacements.

4.2. Semiconductor lasers

In a recent chapters we presented an application of photoreflectance spectroscopy to investigation of such microstructures like quantum wells, wires, dots and transistor structures. Using PR, we are able to study even more complicated multi-layer structures. In this chapter, we present some examples of PR studies of laser structures.

The vertical cavity surface emitting laser (VCSEL) became recently very important for opto-electronics. VCSEL

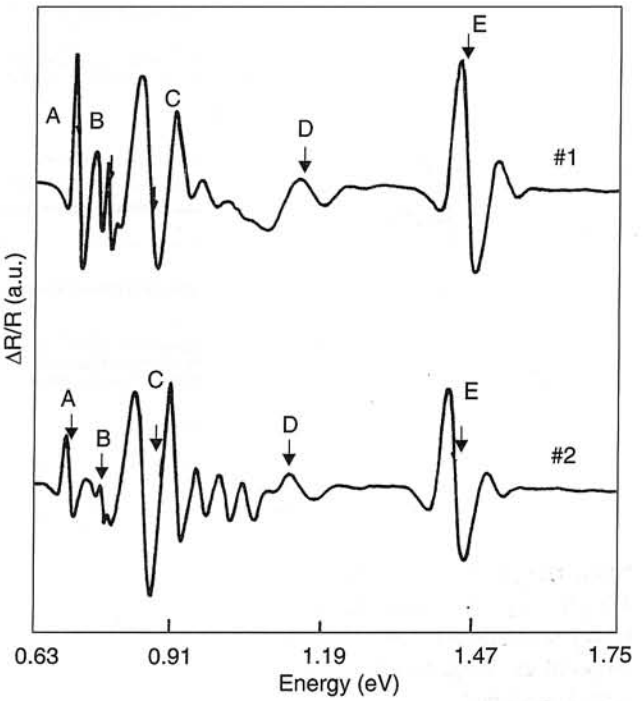

Fig. 26. The photoreflectance spectra from InAlAs/InGaAs HBTs with 30 nm (#1) and 50 nm (#2) spacer thickness. The origin of marked with arrows optical transitions is described in text (after Ref. 49).

has several advantageous properties such as single longitudinal mode operation, small beam divergence, low threshold current and ease of integrability. The photoreflectance results on VCSEL structures were reported by Berger et al. [54,55]. Samples were grown by gas source MBE. The structures consisted of an n^+ distributed Bragg reflector (DBR) as the bottom mirror, a cavity with three GaAs/AlGaAs QW's and a p^+ DBR as the top mirror (see Fig. 27). The described above full VCSEL structure is marked DU. The structure obtained at the same conditions but without top DBR is marked DT.

Berger *et al.* recorded both the reflected signal RI_0 (not normalised reflectivity) and the modulated signal ΔRI_0. A numerical division of ΔRI_0 by RI_0 gave the PR spectra. Obtained at room temperature reflected spectra and PR spectra for full structure (DU) and the structure without top DBR (DT) are plotted in Fig. 28. Dashed lines represent the RI_0 signal. For DU structure, the RI_0 signal shows a reflectivity plateau of the cavity. Near 1.58 eV, RI_0 exhibits a slight dip, which is due to the resonance (Fabry-Perot) mode of the cavity. Solid lines represent PR spectra. The PR spectra in Fig. 28 exhibit two groups of features in each structure. An attributed to the quantum well transition occurs around 1.5 eV. Between 1.6 and 1.7 eV is a feature related to the AlGaAs layers. In the energy range of the plateau, both features in the DU spectrum are screened. Therefore, it is not possible to precisely determine the transition energies from this spectrum. The PR spectrum for the DT structure was used to determine the transition energies in the DU spec-

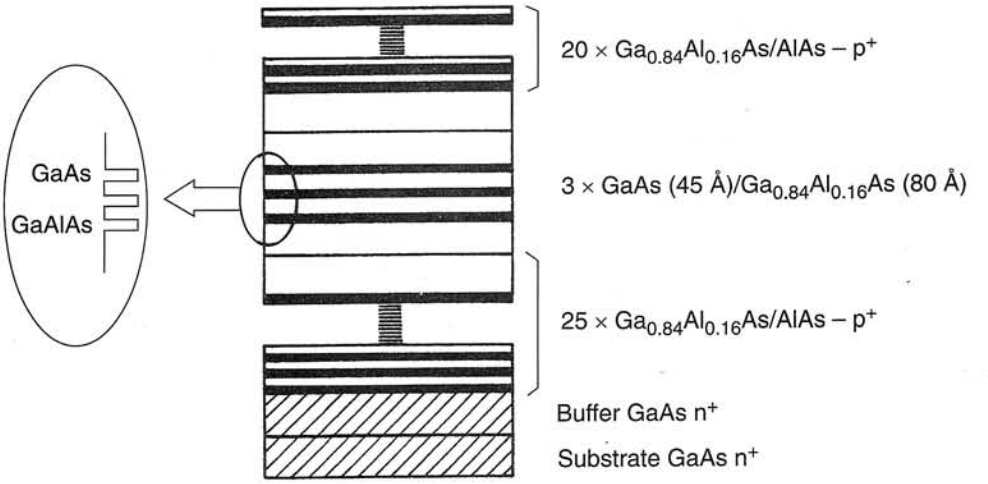

Fig. 27. Schematic diagram of the GaAs/(AlGa)As based VCSEL structure (after Ref. 55).

trum. Berger *et al.* has discovered that the features about 1.5 eV originates from the optical transition between the heavy hole and the electron subbands. From the energy position of the AlGaAs related feature, the Al content of 16% was determined.

In order to change the quantum well transition energy, the measurements were performed at temperatures down to 9 K. The PR and RI_0 spectra for full VCSEL structure obtained at 300 K, 110 K and 9 K are shown in Fig. 29. In the PR spectra, the AlGaAs related transitions exhibits Franz-Keldysh oscillations, from which the value of the electric field in the cavity is 38 kV/cm at room temperature and decreases to 17 kV/cm at 9 K. At lower temperatures, the AlGaAs related transitions are no more screened. As the temperature decreases, the energy shift of QW transition is larger than the Fabry-Perot cavity mode shift. The intensity of the PR feature corresponding to the 11H transition is arising as temperature decreases. The maximum intensity was observed at 110 K. Two features around 1.57 eV are present in the spectrum corresponding to temperature 110 K. The higher energy feature originates from the 11H transition and the lower energy feature corresponds to the Fabry-Perot cavity mode [55].

Klar *et al.* [56,57] performed photoreflectance and conventional reflectance studies on an InGaAs/GaAs/AlGaAs vertical cavity surface emitting laser structure at room temperature. The structure was grown by MBE on GaAs n^+ substrate. It was designed for operation at $\lambda = 1$ μm, and consists of a GaAs cavity with an 8.5 nm wide, compressively strained $In_{0.28}Ga_{0.72}As$ quantum well in the centre. The cavity is embedded between bottom (n^+) and top (p^+) distributed Bragg reflectors.

Figure 30 shows set of room temperature PR spectra, for different angles of incidence of the probe light. The spectra were taken with the lock-in amplifier set to detect $\Delta R/R$ signal, in-phase with respect to the constant PL background from the sample [56]. All the photoreflectance spectra show three prominent features. The first, at about 1.185 eV is 11H exciton transition in the $In_{0.28}Ga_{0.72}As$ quantum well. The second signal moves to higher energy with increasing angle of incidence. It shows the same angular dependence as the cavity mode in the reflectivity spectrum, hence Klar *et al.* conclude that this PR signal is due to the modulation of the cavity mode. Due to a variation in the In concentration, the ground-state QW transition is

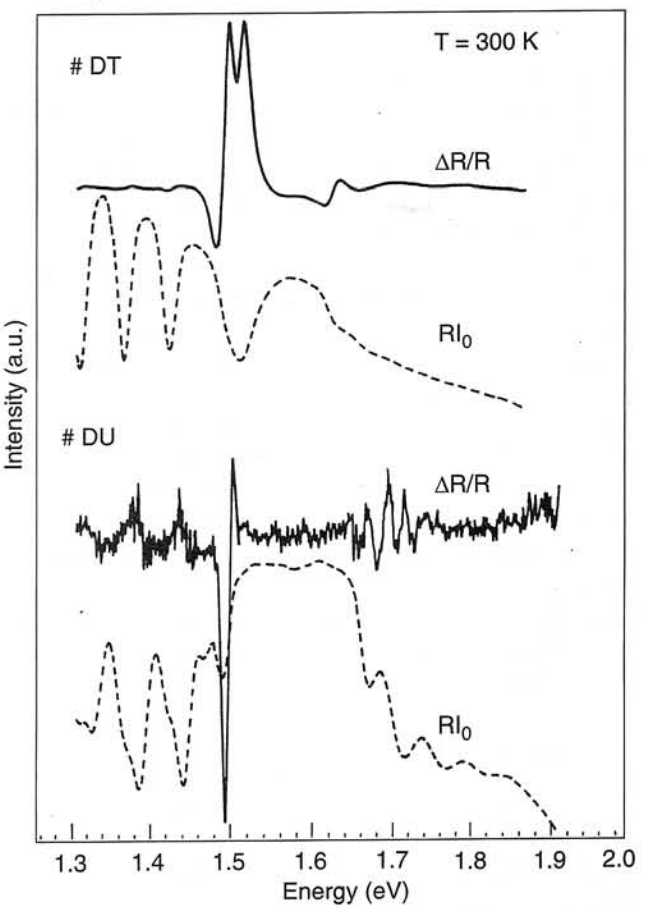

Fig. 28. Photoreflectance spectra at 300 K from the full VCSEL structure (#DU) and structure without distributed Bragg reflector (#DT) – solid lines. Dashed lines represent reflected signal – RI_0 (after Ref. 54).

 © 2000 COSiW SEP, Warsaw

about 100 meV lower in energy than the cavity mode. The third signal, above 1.4 eV, is due to Franz-Keldysh oscillations in the GaAs layers.

The strength of the signal from the cavity mode varies with angle of incidence and is stronger between 30° and 60°, than at angles of 15° and 75°. This may be explained as follows. When the cavity mode feature overlaps in energy with higher-order quantum well transition, probe light at this energy will be more strongly modulated by the QW than at other angles of incidence (such as 15° and 75°). Thus, one would expect to observe a stronger photoreflectance signal for cavity mode when it passes through positions of resonance with the higher-order QW transition, which are 12H, 13H, 21H and 22H for QW being under study [56]. For the ranges of incidence between 30° and 60° the cavity mode passes through 13H and 21H resonances.

The origin and lineshape of the photoreflectance signal associated with cavity mode, Klar et al. explained as follows [56]. Due to the modulation-induced changes in the complex refractive index of the cavity layers, the cavity mode feature in the reflectance spectrum gives rise to corresponding feature in the photoreflectance. Thus, the PR lineshape of this feature corresponds to the first derivative of the cavity mode dip in the reflectance spectrum.

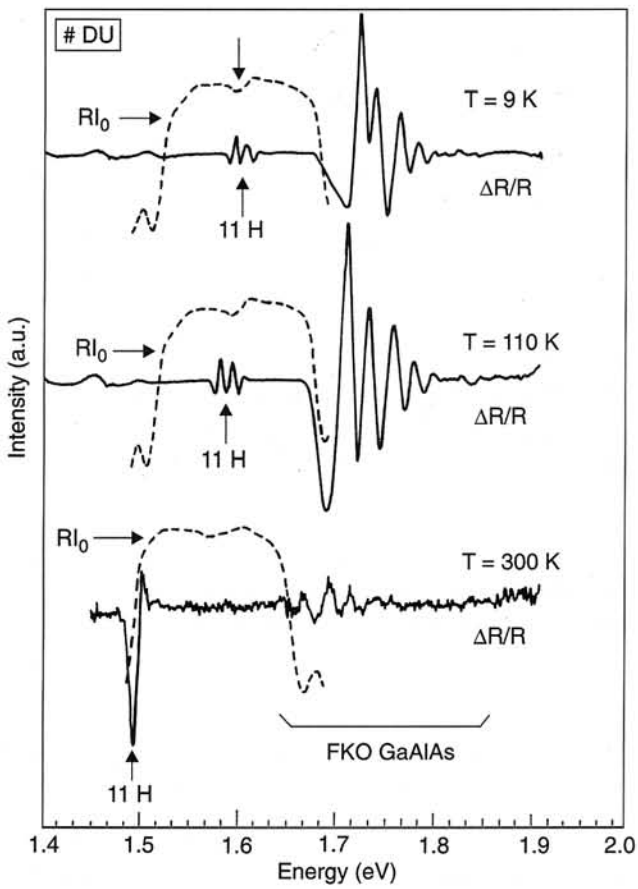

Fig. 29. Photoreflectance spectra from the full structure of a VCSEL (#DU) at 300 K, 110 K and 9 K (solid lines). Dashed lines hold for reflected signal (after Ref. 54).

Klar *et al.* continued studies of InGaAs/GaAs/ AlGaAs VCSEL structure, measuring the photoreflectance spectra at hydrostatic pressures up to 1.24 GPa [57]. Figure 31 shows a series of photoreflectance spectra for various hydrostatic pressures. All the spectra show two signals. At ambient pressure, low-energy signal, at about 1.19 eV, can be assigned to the 11H transition. High-energy signal, at about 1.295 eV is attributed to the cavity mode. Both signals shift towards higher energy with increasing pressure. Because the energy shift of quantum well exciton feature is bigger than that of cavity mode feature, at the highest pressure, the overlap between those two features is observed.

From photoreflectance data, Klar *et al.* calculated the pressure coefficients for the QW exciton and the cavity mode, which are 92 meV/GPa and 15 meV/Gpa, respectively. The pressure coefficient for 11H transition is in agreement with studies of strained InGaAs QWs embedded in GaAs barriers. Klar *et al.* found that the value of pressure coefficient for the cavity mode is mainly caused by the pressure-induced change of the refractive index of the cavity.

Berger *et al.* [54,55] and Klar *et al.* [56,57] demonstrated that the photoreflectance spectroscopy can be a powerful tool for studies of the gain and loss mechanisms in VCSEL devices.

Pollak *et al.* [58] investigated multiple quantum well planar emitting laser structures. They performed a room temperature PR study of two pseudomorphic InGaAsP/InP 1.3 μm MQW laser structures. The structures were fabri-

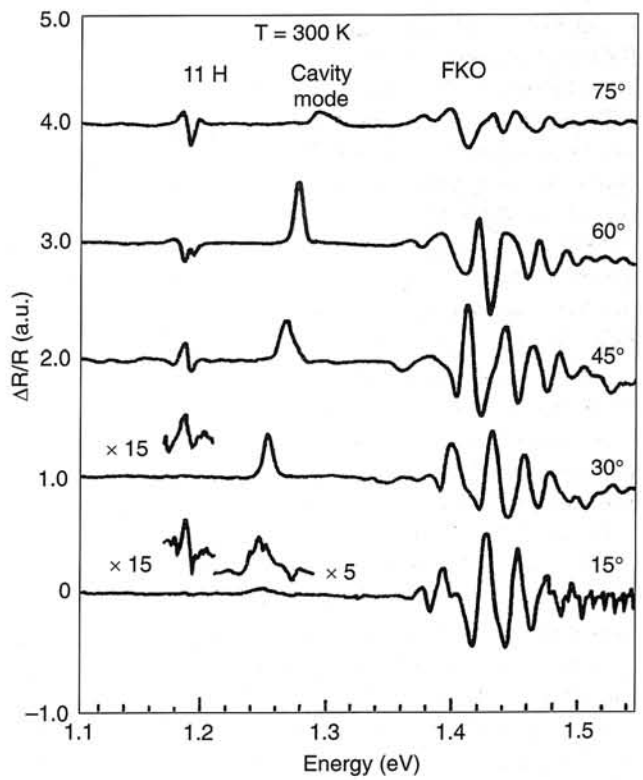

Fig. 30. Photoreflectance spectra from InGaAs/GaAs/AlGaAs VCSEL structure for different angles of incidence of the probe light (values indicated on the right) taken at room temperature (after Ref. 56).

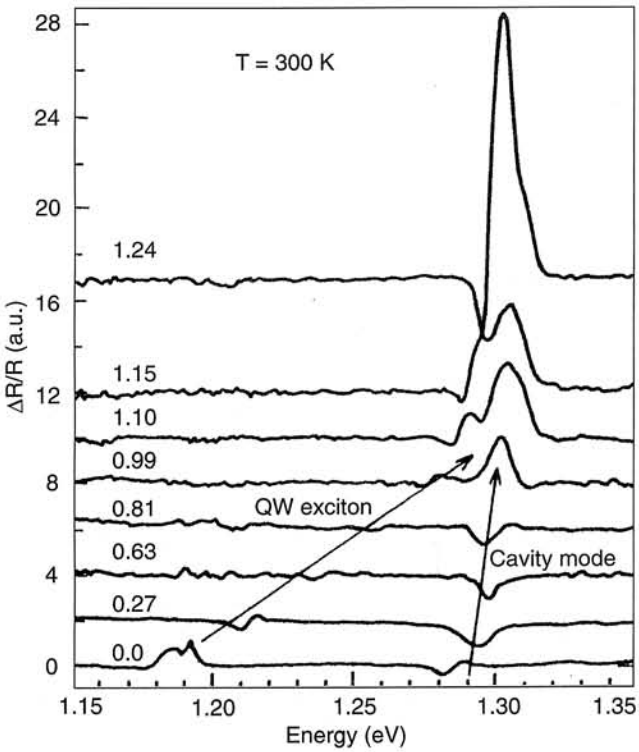

Fig. 31. Photoreflectance spectra from InGaAs/GaAs/AlGaAs VCSEL structure for various hydrostatic pressures. The pressure values in GPa are indicated on the left of the spectra (after Ref. 57).

cated by MOCVD technique. The first structure was grown on a (001) InP substrate with an InP n^+ buffer. A lattice-matched separate confinement heterostructure (SCH) InGaAsP of about 50 nm thick, followed by 6-10 strained layer InGaAsP QWs with lattice-matched InGaAsP barriers was grown on the buffer layer. The MQW stack was followed by another lattice-matched InGaAsP SCH and by an InP p^+ layer. The entire structure was covered with a lattice-matched InGaAsP cap.

Figure 32 presents the room temperature PR spectrum of a structure with 6 nm QWs. The features below 1.1 eV originate from the MQW stack. The signal above 1.3 eV comes from the top InP p^+ layer. The feature exhibits Franz-Keldysh oscillations, which can be used to find information about the built-in electric field in this region. Between these two groups of features is a Franz-Keldysh oscillation originating from the SCH. The built-in SCH region's electric field is about 41 kV/cm. The band gap of SCH material is 1.104 eV, which means that materials are lattice-matched.

A lineshape fit made it possible to accurately determine the energies of five quantum transitions in the MQW. The lowest energy feature is due to the 11H optical transition. This transition is responsible for the lasing frequency of the structure. The energy of 11H transition is 0.925 eV (1.34 μm).

Aigouy *et al.* [59] evaluated the energy of the fundamental transition (11H) in a 0.98 μm InGaAs/ GaAs/InGaP p-i-n quantum well laser, as a function of both, the bias applied to the laser, and the position on the laser stripe. They used both, photoreflectance and electroreflectance techniques with a spatial resolution of about 10 μm. The laser device was grown by MOCVD on an n^+ GaAs (001) substrate. The active region consisted of two undoped pseudomorphic 7-nm $In_{0.19}Ga_{0.81}As$ QWs separated by a 20-nm undoped GaAs barrier. The active region was surrounded on each side by 85 nm of GaAs, sandwiched between n- and p-type InGaP.

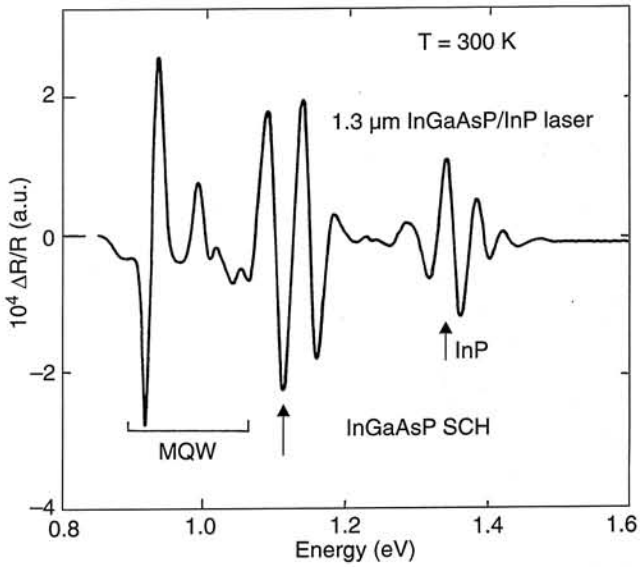

Fig. 32. Photoreflectance spectrum from a pseudomorphic 1.3 μm InGaAsP/InP MQW laser structure with QWs width of 6 nm (after Ref. 58).

The application of a forward bias results in a blue shift in the 11H transition energy, a decrease in the line width and an increase in the amplitude of the spectral feature. Reverse bias has the opposite effect. These changes in various parameters are a consequence of the quantum confined Stark effect. At zero bias, the QWs are in the electric field of the p-i-n structure. Application of the bias changes the electric field, which causes a shift of the transition energy and changes of other parameters. Aigouy *et al.* evaluated the electric field to be 70 kV/cm at a zero bias.

Aigouy *et al.* performed a scan of the 11H transition energy versus the localisation of the probe light spot on the surface of laser structure. They scanned a surface of 750×50 μm and found spatial variations in the 11H transition energy of 6–7 meV over the entire region. These spatial variations are probably due to inhomogeneities in composition and the electric field distribution.

5. Conclusions

In this review paper, we presented the applications of photoreflectance spectroscopy for investigations of low-dimensional, semiconductor structures. The theoretical background of this technique including the line-shape expressions for photoreflectance spectra related to semiconductor microstructures, was briefly introduced.

In the first part of our work, we presented the exemples of photoreflectance spectroscopy investigations of quantum

 © 2000 COSiW SEP, Warsaw

wells, multiple quantum wells, superlattices, quantum wires and quantum dots. In the second part we concentrated on the investigations of semiconductor device structures such as transistors and semiconductor lasers.

Photoreflectance, which is the contactless modulation spectroscopy technique can be carried out even at room temperature, providing as much information as other optical methods (PL, PLE) at very low temperatures.

The examples we have shown confirm that the photoreflectance is appropriate for the investigations of both semiconductor low-dimensional structures and device structures.

Acknowledgements

This work was partially supported by the Centre for Advanced Materials and Nanotechnology, Wrocław University of Technology.

References

1. O.J. Glembocki, B.V. Shanbrook, N. Bottka, W.T. Beard, and J. Comas, "Photoreflectance characterisation of interband transitions in GaAs/AlGaAs multiple quantum wells and modulation-doped heterojunctions", *Appl. Phys. Lett.* **46**, 970–972 (1985).
2. O.J. Glembocki and B.V. Shanabrook, "Photoreflectance spectroscopy of microstructures", in *Semiconductors and Semimetals*, Vol. **36**, pp. 221–292, edited by D.G. Seiler and C.L. Littler, Academic Press, New York, 1992.
3. F.H. Pollak and O.J. Glembocki, "Modulation spectroscopy of semiconductor microstructures: an overview", *Proc. SPIE* **946**, 2–35 (1988).
4. F.H. Pollak, H. Qiang, D. Yan, Y. Yin, and V.T. Boccio, "Better device yields with modulation spectroscopy", *Photonics Spectra* **27**, 78–84 (1993).
5. F.H. Pollak, "Modulation spectroscopy of semiconductors and semiconductor microstructures", in *Handbook on Semiconductors*, Vol. 2, pp. 527–635, edited by M. Balkanski, Elsevier Science B.V., Amsterdam, 1994.
6. O.J. Glembocki, "Modulation spectroscopy of semiconductor materials, interfaces, and microstructures: an overview", *Proc. SPIE* **1286**, 2–30 (1990).
7. P.J. Klar, C.M. Townsley, D. Wolverson, J.J. Davies, D.E. Ashenford, and B. Lunn, "Photomodulated reflectivity of $Zn_{1-x}Mn_xTe$/ZnTe multiple-quantum wells with below-bandgap excitation", *Semicond. Sci. Technol.* **10**, 1568–1577 (1995).
8. B.O. Seraphin and N. Bottka, "Band-structure analysis from electro-reflectance studies", *Phys. Rev.* **145**, 628–636 (1966).
9. D.E. Aspnes, "Third-derivative modulation spectroscopy with low-field electroreflectance", *Surface Science* **37**, 418–442 (1973).
10. D.E. Aspnes, "Electric field effects on the dielectric constant of solids", *Phys. Rev.* **153**, 972–982 (1967).
11. D.E. Aspnes, "The dielectric function of semiconductors", in *Handbook on Semiconductors*, Vol. 2, pp. 110–154, edited by M. Balkanski, North-Holland, Amsterdam, 1980.
12. B.V. Shanabrook, O.J. Glembocki, and W.T. Beard, "Photoreflectance modulation mechanisms in GaAs-$Al_xGa_{1-x}As$ quantum wells", *Phys. Rev.* **B35**, 2540–2543 (1987).
13. Y.S. Huang, H. Qiang, F.H. Pollak, J. Lee, and B. Elman, "Electroreflectance study of a symmetrically coupled GaAs/$Ga_{0.77}Al_{0.23}As$ double quantum well system", *J. Appl. Phys.* **70**, 3808–3814 (1991).
14. D.E. Aspnes, and A.A. Studna, "Schottky-barrier electroreflectance: Application to GaAs", *Phys. Rev.* **B7**, 4605–4625 (1973).
15. D.E. Aspnes, "Band nonparabolicities, broadening, and internal field distributions: The spectroscopy of Franz-Keldysh oscillations", *Phys. Rev.* **B10**, 4228–4238 (1974).
16. M. Cardona, *Modulation Spectroscopy*, Academic Press, New York, 1969.
17. O.J. Glembocki and B.V. Shanabrook, *Proc. SPIE* **794**, 12 (1987).
18. P. Sitarek, G. Sek, J. Misiewicz, and T.S. Cheng, "Investigations of allowed and forbidden transitions in (AlGa)As/GaAs multiple quantum wells", *Vacuum* **50**, 203–205 (1998).
19. P. Sitarek, G. Sęk, J. Misiewicz, and T.S. Cheng, "Above-barrier states investigations in (AlGa)As/GaAs quantum structures by using photoreflectance spectroscopy", *Institute of Physics* U.K. **152**, 657–660 (1998).
20. G. Bastard, *Wave Mechanics Applied to Semiconductor Heterostructures*, Les Editions de Physique, Paris, 1992.
21. J.E. Zucker, A. Pinczuk, D.S. Chemla, A.C. Gossard, and W. Wiegmann, "Delocalised excitons in semiconductor heterostructures", *Phys. Rev.* **B29**, 7065–7068 (1984).
22. J.J. Song, Y.S. Yoon, A. Fedorowsky, Y.B. Kim, J.N. Schulman, C.W. Tu, D.M. Huang, and H. Morkoc, "Barrier-width dependence of optical transitions involving unconfined energy states in GaAs-$Al_xGa_{1-x}As$ superlattices", *Phys. Rev.* **B34**, 8958–8962 (1986).
23. U.K. Reddy, G. Ji, T. Henderson, H. Morkoç, and J.N. Schulman, "Investigation of GaAs/(Al,Ga)As multiple quantum wells by photoreflectance", *J. Appl. Phys.* **62**, 145–151 (1987).
24. G. Ji, W. Dobbelaere, D. Huang, and H. Morkoç, "Optical transitions involving unconfined energy states in $In_xGa_{1-x}As$/GaAs multiple quantum wells", *Phys. Rev.* **B39**, 3216–3222 (1989).
25. H. Shen, S.H. Pan, Z. Hang, F.H. Pollak, and R.N. Sacks, "Miniband dispersion of the confined and unconfined states of coupled multiple quantum wells", *Solid State Commun.* **65**, 929–934 (1988).
26. S.H. Pan, H. Shen, Z. Hang, F.H. Pollak, W. Zhuang, Q. Xu, A.P. Roth, R.A. Masut, C. Lacelle, and D. Morris, "Photoreflectance study of narrow-well strained-layer $In_xGa_{1-x}As$/GaAs coupled multiple-quantum-well structures", *Phys. Rev.* **B38**, 3375–3382 (1988).
27. G. Sęk, J. Misiewicz, D. Radziewicz, M. Tłaczała, M. Panek, and R. Korbutowicz, "Study of the nature of light hole excitonic transitions in InGaAs/GaAs quantum well", *Vacuum* **50**, 199–201 (1998).
28. P. Sitarek, J. Misiewicz, G. Karczewski, T. Wojtowicz, and J. Kossut, "CdTe/$Cd_{1-x}Mn_xTe$ quantum structures investigated by photoreflectance spectroscopy", *Electron Technology* **31**, 311–313 (1998).
29. G. Sęk, K. Ryczko, M. Kubisa, J. Misiewicz, J. Koeth, and A. Forchel, "Photoreflectance study of coupling effects in double quantum wells", *Opto-Electr. Rev.* **7**, 117–119 (1999).
30. D. Labrie and J.J. Dubowski, "Evidence for the miniband dispersion in the photoreflectance of a CdTe/$Cd_{1-x}Mn_xTe$ superlattice", *Superlatt. Microstruct.* **16**, 25–28 (1994).

31. Y.S. Tang, C.D.W. Wilkinson, C.M. Sotomayor Torres, D.W. Smith, T.E. Whall, and E.H.C. Parker, "Optical properties of $Si/Si_{1-x}Ge_x$ heterostructure based wires", *Solid State Commun.* **85**, 199–202 (1993).
32. H. Qiang, F.H. Pollak, Y.S. Tang, P.D. Wang, and C.M. Sotomayor Torres, "Characterisation of process-induced strains in $GaAs/Ga_{0.7}Al_{0.3}As$ quantum dots using room-temperature photoreflectance", *Appl. Phys. Lett.* **64**, 2830–2832 (1994).
33. G. Gumbs, D. Huang, H. Qiang, F.H. Pollak, P.D. Wang, C.M. Sotomayor Torres, and M.C. Holland, "Electromodulation spectroscopy of an array of modulation-doped $GaAs/Ga_{1-x}Al_xAs$ quantum dots: Experiment and theory", *Phys. Rev.* **B50**, 10962–10969 (1994).
34. D.P. Wang, C.M. Sotomayor Torres, M.C. Holland, H. Qiang, F.H. Pollak, and G. Gumbs, "Photoreflectance study of modulation-doped GaAs/GaAlAs quantum dots fabricated by reactive-ion etching", *Mat. Res. Soc. Symp. Proc.* **324**, 187–192 (1994).
35. P.J. Klar, D. Wolverson, D.E. Ashenford, B. Lunn, and T. Henning, "Comparison of $Zn_{1-x}Mn_xTe/ZnTe$ multiple-quantum wells and quantum dots by below-bandgap photomodulated reflectivity", *Semicond. Sci. Technol.* **11**, 1863–1872 (1996).
36. C. Ulrich, S. Ves, A.R. Goni, A. Kurtenbach, K. Syassen, and K. Eberl, "Electronic subband structure of $InP/In_xGa_{1-x}P$ quantum islands from high-pressure photoluminescence and photoreflectance", *Phys. Rev.* **B52**, 12212–12217 (1995).
37. G. Sek, J. Misiewicz, K. Ryczko, M. Kubisa, F. Heinrichsdorff, O. Stier, and D. Bimberg, "Room temperature photoreflectance of MOCVD-grown InAs/GaAs quantum dots", *Solid State Commun.* (1999) (in press).
38. G.L. Rowland, T.J.C. Hosea, S. Malik, D. Childs, and R. Murray, "A photomodulated reflectance study of InAs/GaAs self-assembled quantum dots", *Appl. Phys. Lett.* **73**, 3268–3270 (1998).
39. J.A.N.T. Soares, D. Beliaev, R. Enderlein, L.M.R. Scolfaro, M. Saito, and J.R. Leite, "Photoreflectance investigations of semiconductor device structures", *Mater. Sci. Engineer.* **B35**, 267-272 (1995).
40. R. Enderlein, "Photoreflectance studies of (Al,Ga)As/GaAs heterostructures and devices", *Phys. Stat. Sol. (b)* **194**, 257–277 (1996).
41. G. Sęk, J. Misiewicz, and T.S. Cheng, „Photoreflectance spectroscopy of low-dimensional GaAs/AlGaAs structures", *Adv. Mater. Opt. Electron.* **7**, 241–247 (1997).
42. Y. Yin, H. Qiang, F.H. Pollak, D.C. Streit, and M. Wojtowicz, "Two-dimensional electron gas effects in the electromodulation spectra of a pseudomorphic $Ga_{0.78}Al_{0.22}As/In_{0.21}Ga_{0.79}As/GaAs$ modulation-doped quantum well structure", *Appl. Phys. Lett.* **61**, 1579–1581 (1992).
43. Y. Yin, H. Qiang, D. Yan, F.H. Pollak, and T.F. Noble, "Room-temperature photoreflectance characterization of pseudomorphic GaAlAs/ InGaAs/GaAs high electron mobility transistor structures including the two-dimensional electron gas density", *Semocond. Sci. Technol.* **8**, 1599–1604 (1993).
44. A.C. Han, M. Wojtowicz, D. Pascua, T.R. Block, and D.C. Streit, "Photoreflectance study of pseudomorphic high electron mobility transistors", *J. Appl. Phys.* **82**, 2607–2610 (1997).
45. W. Liu, D. Jiang, Y. Zhang, S. Jin, and R. Wang, "Spectroscopic studies of the effects of two-dimensional electron gas on interband transitions", *J. Appl. Phys.* **77**, 4564–4567 (1995).
46. N. Bottka, D.K. Gaskill, P.D. Wright, R.W. Kaliski, and D.A. Wiliams, "Qualification of OMVPE AlGaAs/GaAs HBT structures using nondestructive photoreflectance spectroscopy", *J. Cryst. Growth* **107**, 893–897 (1991).
47. W.D. Sun, and F.H. Pollak, "On the origins of the Franz-Keldysh oscillations observed in the electromodulation spectra of graded emitter $Ga_{1-x}Al_xAs/GaAs$ heterojunction bipolar transistor structures", *J. Appl. Phys.* **83**, 4447–4453 (1998).
48. D. Yan, F.H. Pollak, V.T. Boccio, C.L. Lin, P.D. Kirchner, J.M. Woodall, R.C. Gee, and P.M. Asbeck, "Photoreflectance characterisation of an InP/InGaAs heterojunction bipolar transistor structure", *Appl. Phys. Lett.* **61**, 2066–2068 (1992).
49. K.T. Hsu, Y.H. Chen, K.L. Chen, H.H. Lin, and G.J. Jan, "Photoreflectance characterisation of an InAlAs/InGaAs heterostructure bipolar transistor", *Appl. Phys. Lett.* **64**, 1974–1976 (1994).
50. Y.H. Chen, K.T. Hsu, K.L. Chen, H.H. Lin, and G.J. Jan, "Room-temperature photoreflectance characterisation of InAlAs/InGaAs heterojunction bipolar transistor structure including two-dimensional electron gas", *Jpn. J. Appl. Phys.* **33**, 2448–2452 (1994).
51. Y.H. Chen and G.J. Jan, "Photoreflectance study on the two-dimensional electron gas of InAlAs/InGaAs heterojunction bipolar transistor grown by molecular beam epitaxy", *J. Appl. Phys.* **77**, 6681–6685 (1995).
52. Y.H. Chen and G.J. Jan, "Photoreflectance characterization on the InAlAs-InGaAs heterojunction bipolar transistors", *IEEE J. Quantum Electron.* **33**, 574–578 (1997).
53. K.L. Chen, H.H. Lin, G.J. Jan, Y.H. Chen, and P.K. Tseng, "Photoreflectance temperature dependence of graded InAlAs/InGaAs heterojunction bipolar transistor layers", *J. Appl. Phys.* **78**, 4035–4038 (1995).
54. P.D. Berger, C. Bru, T. Benyatou, A. Chenevas-Paule, and P. Grosse, "Investigations of VCSEL resonant cavities by photoreflectance spectroscopy", *Proc. SPIE* **2397**, 726–732 (1995).
55. P.D. Berger, C. Bru, T. Benyatou, G. Guillot, A. Chenevas-Paule, L. Couturier, and P. Grosse, "Investigations of vertical cavity surface emitting laser by photoreflectance spectroscopy", *Appl. Phys. Lett.* **68**, 4–6 (1996).
56. P.J. Klar, G. Rowland, T.E. Sale, T.J.C. Hosea, and R. Grey, "Reflectance and photomodulated reflectance studies of cavity mode and excitonic transitions in an InGaAs/GaAs/AlAs/AlGaAs VCSEL structure", *Phys. Stat. Sol. (a)* **170**, 145–158 (1998).
57. P.J. Klar, P.M.A. Vincente, T.E. Sale, T.J.C. Hosea, A.R. Adams, and A. Raymond, "Reflectance and photomodulated reflectance studies of an InGaAs/GaAs/AlGaAs vertical-cavity surface- -emitting laser structure under hydrostatic pressure", *Solid State Commun.* **107**, 97–100 (1998).
58. F.H. Pollak, W. Krystek, M. Leibovitch, L. Malikova, M.S. Hybertsen, R. Lum, J.M. Vandenberg, and C.L. Reynolds, "Room temperature, contactless electromodulation investigation of wafer-sized quantum well laser structures", *Proc. SPIE* **2693**, 455–466 (1996).
59. L. Aigouy, F.H. Pollak, and G. Gumbs, "Micro-electroreflectance and photoreflectance characterisation of the bias dependence of the quantum confined Stark effect in a fabricated 0.98 μm InGaAs/GaAs/InGaP laser", *Appl. Phys. Lett.* **70**, 2562–2564 (1997).

 © 2000 COSiW SEP, Warsaw